

DETECTION AND CHARACTERIZATION OF EXTRASOLAR PLANETS THROUGH DOPPLER SPECTROSCOPY

A. Eggenberger¹ and S. Udry²

Abstract. Over 300 extrasolar planets have been found since 1992, showing that planetary systems are common and exhibit an outstanding variety of characteristics. As the number of detections grows and as models of planet formation progress to account for the existence of these new worlds, statistical studies and confrontations of observation with theory allow to progressively unravel the key processes underlying planet formation. In this chapter we review the dominant contribution of Doppler spectroscopy to the present discoveries and to our general understanding of planetary systems. We also emphasize the synergy of Doppler spectroscopy and transit photometry in characterizing the physical properties of transiting extrasolar planets. As we will see, Doppler spectroscopy has not reached its limits yet and it will undoubtedly play a leading role in the detection and characterization of the first Earth-mass planets.

1 Introduction

The question of the existence of other worlds has been present in human history for millennia but it is only recently that scientific evidence has confirmed what many had anticipated: planets do exist and are common outside the Solar System. The first robust detection of another planetary system came in 1992 with the discovery of two terrestrial-mass planets orbiting the pulsar PSR 1257+12 (Wolszczan & Frail 1992). Interestingly, this discovery did not receive all the attention that could have been expected, probably because these two planets orbit

We warmly thank the organizers for their invitation. We thank Olivier Preis for comments that helped improve the quality of the manuscript. A. E. acknowledges support from the French National Research Agency through project grant ANR-NT-05-4_44463.

¹ Laboratoire d'Astrophysique de Grenoble, UMR 5571 CNRS/Université Joseph Fourier, BP 53, F-38041 Grenoble Cedex 9, France; e-mail: Anne.Eggenberger@obs.ujf-grenoble.fr

² Observatoire de Genève, Université de Genève, 51 ch. des Maillettes, CH-1290 Sauverny, Switzerland; e-mail: Stephane.Udry@unige.ch

a “dead star” very different from the Sun and much less likely to host life in its vicinity. From this anthropocentric perspective, the major milestone in the search for extrasolar planets was the discovery in 1995 of 51 Peg b, the first extrasolar planet found to orbit a Sun-like star (Mayor & Queloz 1995). Although of Jovian nature, 51 Peg b orbits at 0.052 AU from its parent star, a striking characteristic when compared to the giant planets in the Solar System, which all orbit beyond 5 AU. This proximity has been a major surprise and a serious challenge to planet formation theories.

Thirteen years after the discovery of 51 Peg b, over 300 extrasolar planets have been detected, including many fascinating systems¹. Five different techniques have contributed to these discoveries: pulsar timing (4 planets detected; e.g. Wolszczan 1997), Doppler spectroscopy (292 planets; e.g. Udry et al. 2007), photometric transits (52 planets; e.g. Charbonneau et al. 2007), microlensing (8 planets; e.g. Gaudi 2007), and direct imaging (4 objects with a mass possibly below $20 M_{\text{Jup}}$; e.g. Beuzit et al. 2007). These observational techniques have considerably improved in recent years and Doppler spectroscopy, which has contributed the bulk of the discoveries so far, now allows the detection of planets with half the mass of Uranus.

Likewise, since the discovery of 51 Peg b, planet formation theory has made rapid progress. To overcome the challenge posed by the unexpected properties of the newly found planets, two different formation models have been proposed: core accretion and disk instability. According to the core accretion model, dust grains coagulate to form planetesimals, which then accumulate to build up planetary cores. Planetary cores reaching the critical mass of 5-15 M_{\oplus} before the dissipation of the gaseous protoplanetary disk subsequently accrete significant amounts of nebular gas and become giant planets (e.g. Lissauer & Stevenson 2007). The remaining solid cores merge through giant impacts to form terrestrial planets (e.g. Nagasawa et al. 2007). In the alternative disk instability model, giant planets form by direct fragmentation of the protoplanetary disk (e.g. Durisen et al. 2007). Quantitative predictions based on the disk instability scenario are still sparse because the simulations are computationally challenging and involve complex physics. In contrast, core accretion is now mature enough to allow for detailed calculations, and explicit comparisons with the observed population of extrasolar planets are possible.

In this chapter we review the dominant contribution of Doppler spectroscopy to planet discoveries and to our general understanding of planetary systems. In Sect. 2 we describe the Doppler technique itself. Then, we present the observational results and we discuss their interpretation within the current theoretical framework. In Sect. 3 we consider the results on giant planets for which an extended statistics is available. In Sect. 4 we present recent results on low-mass planets of Neptune- and Earth-type, and we discuss the present limitations on Doppler precision. We end this review by describing in Sect. 5 the role played by Doppler spectroscopy in the characterization of transiting planets. All these

¹See the Extrasolar Planets Encyclopedia, <http://exoplanet.eu/>, for an up-to-date census of the discoveries.

achievements and results are summarized in Sect. 6, where we also outline future perspectives.

2 Doppler spectroscopy

2.1 Principle

Doppler spectroscopy is an indirect detection method which uses the starlight to measure the gravitational influence of a planet on its host star. Specifically, Doppler spectroscopy is based on the following key observations:

1. In a planetary system, the star and the planet orbit their common barycenter according to Newton's law of gravitation and to the laws of motion. The two barycentric and the relative orbits have the same periods and eccentricities, but semimajor axes in the proportions $a_* : a_p = m_p : m_* : (m_* + m_p)$, where m_* is the mass of the parent star and m_p the mass of the planet. The three orbits are coplanar and the orientations of the two barycentric orbits differ by 180° within that plane.
2. According to the Doppler-Fizeau effect (hereafter simply the Doppler effect), the light emitted by a source approaching (receding from) the observer is shifted towards shorter (longer) wavelengths. In its simplest relativist form, the Doppler formula writes

$$z = \frac{\lambda - \lambda_0}{\lambda_0} = \frac{1 + V_r/c}{\sqrt{1 - V^2/c^2}} - 1 \quad (2.1)$$

where z is the so-called redshift, λ and λ_0 are the observed and rest wavelengths, respectively, V_r is the radial velocity, and V is the total velocity relative to the observer. In the $\ln \lambda$ space, the wavelength shift is independent of the rest wavelength and provides a direct measurement of the relative velocity between the source and the observer.

3. The visible portion of the spectra of F, G, K and M dwarfs contains a multitude of metal absorption lines (Fig. 1). These lines constitute a convenient benchmark to measure wavelength shifts through the Doppler effect.

Putting these three observations together, Doppler spectroscopy consists in monitoring potential Doppler shifts in the spectra of stars with numerous absorption lines. In the absence of other phenomena susceptible of shifting the stellar lines or of modifying their profile (Sect. 2.4.2), measured Doppler shifts are converted into radial (line-of-sight) velocity variations and interpreted as the reflex motion of the star due to an orbiting companion (planet, brown dwarf, or star). Since the two barycentric and the relative orbits are closely related, measuring the reflex motion of the parent star along the line of sight gives access to some of the orbital parameters and characteristics of the companion.

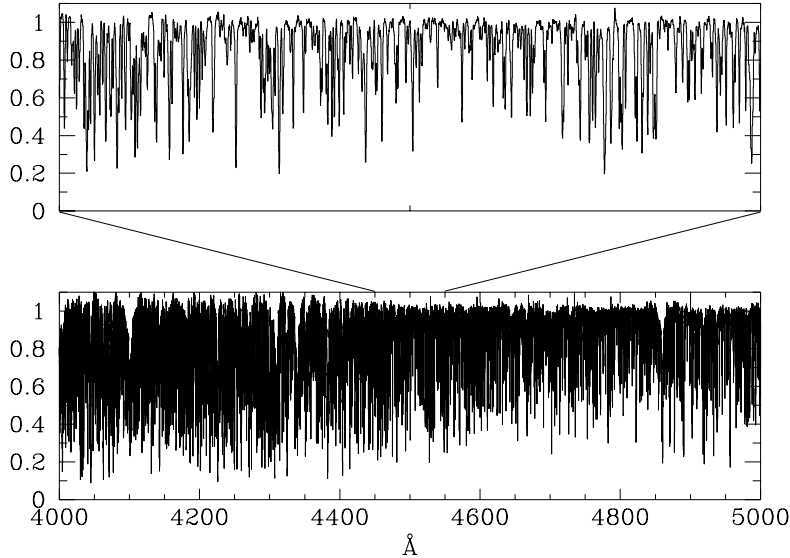


Fig. 1. Blue part of an ELODIE spectrum of the planet-host star 51 Peg illustrating the multitude of absorption lines present in the visible spectra of solar-type stars.

2.2 Planetary orbits and planet characteristics from radial velocities

A planet in a Keplerian orbit induces on its parent star a perturbation of the form

$$V_r(t) = K [\cos(\nu(t) + \omega) + e \cos(\omega)] + \gamma \quad (2.2)$$

where K is the velocity semi-amplitude

$$K = \frac{2\pi a_\star \sin i}{P(1 - e^2)^{1/2}} \quad (2.3)$$

ω is the longitude of periastron, and γ is the systemic velocity (velocity of the barycenter). Since the true anomaly, $\nu(t)$, depends on the orbital period (P), eccentricity (e) and time of passage at periastron (T_0), fitting a radial-velocity time series with the Keplerian model described above yields six parameters: K , e , w , T_0 , P , and γ (Fig. 2).

For a planetary system, the velocity semi-amplitude is related to the masses of the two components through the so-called mass function

$$\frac{(m_p \sin i)^3}{(m_\star + m_p)^2} = \frac{P}{2\pi G} K^3 (1 - e^2)^{3/2} \quad (2.4)$$

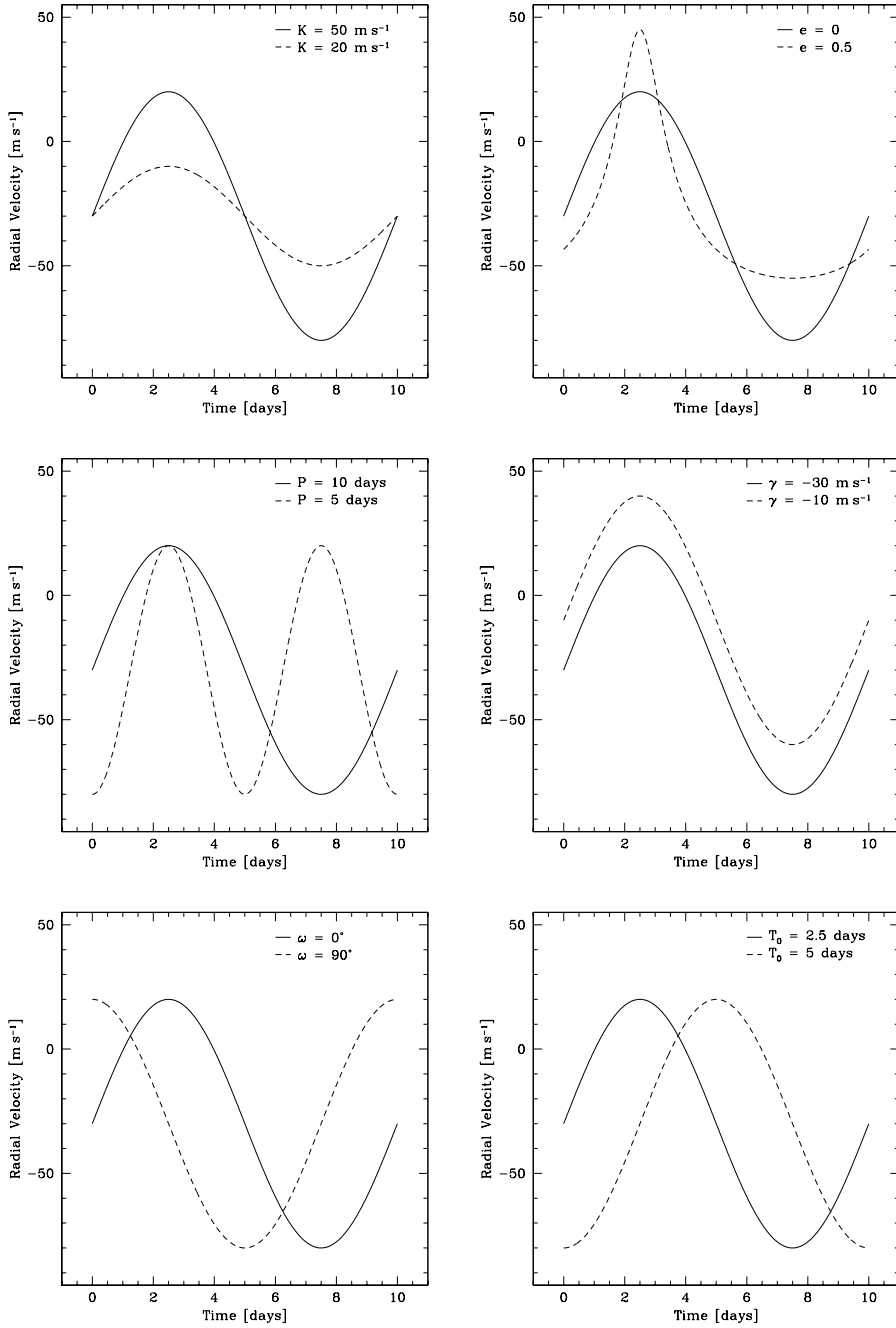


Fig. 2. Illustration of the influence of each of the six parameters determining the Keplerian model of Eq. 2.2. The baseline model has $P = 10 \text{ days}$, $e = 0$, $K = 50 \text{ m s}^{-1}$, $\omega = 0^\circ$, $T_0 = 2.5 \text{ days}$, and $\gamma = -30 \text{ m s}^{-1}$. These orbital elements are varied in turn, one on each panel.

which reduces to the expression of the planet minimum mass

$$m_p \sin i \simeq \left(\frac{P}{2\pi G} \right)^{1/3} K m_\star^{2/3} (1 - e^2)^{1/2} \quad (2.5)$$

under the assumption that $m_p \ll m_\star$ (G is the universal gravitational constant). Introducing the same approximation into Kepler's third law yields an expression for the semimajor axis of the relative orbit

$$a \simeq a_p \simeq \left(\frac{G}{4\pi^2} \right)^{1/3} m_\star^{1/3} P^{2/3} \quad (2.6)$$

Therefore, fitting radial-velocity data with a Keplerian model to account for the presence of a planetary companion gives four of the six orbital elements of the relative orbit (the longitude of the ascending node, Ω , and the orbital inclination, i , remain unknown). When the mass of the central star can be estimated by other means, the Keplerian fit additionally yields a lower limit on the planetary mass and the semimajor axis of the relative orbit. Although the true mass of the planet can be significantly different from the minimum mass, the two values agree within a factor of 2 ($m_p \leq 2 m_p \sin i$) in 87% of cases.

For a planet in a circular orbit around a solar-mass star, Eq. 2.5 simplifies to

$$K [\text{m s}^{-1}] \simeq 28.57 m_p \sin i [\text{M}_{\text{Jup}}] P^{-1/3} [\text{yr}] \quad (2.7)$$

Since the probability of detecting a planetary signal depends essentially on the value of the velocity semiamplitude, this expression indicates that Doppler measurements favor the detection of planetary systems with massive and short-period planets. Applied to the Solar System, Eq. 2.7 shows that Jupiter induces on the Sun a radial-velocity perturbation with a semiamplitude of 12.5 m s^{-1} , while the Earth induces a perturbation with a semiamplitude of 9 cm s^{-1} . As we will discuss now, obtaining radial velocities at this level of precision is nontrivial.

2.3 Instrumentation and techniques for high-precision Doppler measurements

A measurement error of 1 m s^{-1} corresponds to $\Delta\lambda/\lambda_0 = 3 \times 10^{-9}$. On the detector of a typical spectrograph ($R \sim 100,000$), this wavelength shift translates into a linear displacement of about 3×10^{-4} resolution element ($\sim 10^{-4}$ line width). Although attaining this precision is feasible by averaging over many spectral lines, experience shows that unless one takes special measures, errors in Doppler measurements are much greater than the above values and are usually systematic (Griffin & Griffin 1973; Brown 1990).

2.3.1 Requirements for high-precision Doppler measurements

Doppler measurements made with spectrometers or classical spectrographs rarely achieve standard errors better than $\sim 200 \text{ m s}^{-1}$ (e.g. Marcy & Benitz 1989; Duquennoy et al. 1991), which falls short of what is needed to detect extrasolar planets. To achieve

the high Doppler precision necessary for the detection of extrasolar planets, the following sources of systematic errors must be addressed:

1. Motion of the photocenter at the spectrograph slit. In Doppler units, the slit width of a spectrograph is typically a few km s^{-1} , meaning that errors larger than 1 m s^{-1} will occur if the photocenter moves away from the slit center by a few 10^{-3} slit widths. In practice, photocenter motions due to guiding errors, focus, seeing fluctuations, and atmospheric refraction usually amount to $\sim 10^{-1}$ slit widths. An efficient solution to this problem is to use an optical fiber (often with the addition of a scrambling device) to convey and scramble the starlight from the telescope to the spectrograph, thereby producing a nearly uniformly illuminated disk at the spectrograph entrance.
2. Variations of air refractive index and thermomechanical flexures. Variations of temperature and barometric pressure modify the refractive index of air near the grating, causing spurious wavelength shifts similar to Doppler shifts. Mechanical instabilities and thermal relaxation also produce non-negligible motions of the spectrum relative to the detector, causing additional spurious shifts and changes in the instrumental profile. For the CORALIE spectrograph, a temperature change of 1 K produces a net velocity drift of $\sim 90 \text{ m s}^{-1}$, while a pressure change of 1 mbar produces a net velocity drift of $\sim 300 \text{ m s}^{-1}$. A partial solution to this problem is to stabilize and control the entire spectrograph in temperature and pressure. Yet, small wavelength shifts cannot be fully avoided and the general way to deal with this problem is to use a simultaneous wavelength calibration to monitor – and then correct for – these “instrumental drifts”.
3. Timing of exposure and barycentric correction. Classical radial velocities are corrected to the Solar System barycenter. The main contributions to the Earth’s barycentric motion are the diurnal rotation of the Earth ($1\text{-}2 \text{ m s}^{-1}$ per minute at most) and the Earth’s orbital revolution ($\pm 30 \text{ km s}^{-1}$ per year). Yet, at the m s^{-1} level, the motion of the Sun around the Solar System barycenter and the motion of the Earth around the Earth-Moon barycenter are also significant. To obtain precise barycentric radial velocities, one thus needs precise Solar System ephemeris and one needs to know the photon-weighted midpoint of each observation to better than 30 s.

The above requirements show that the secret to making high-precision Doppler measurements is to record the wavelength reference spectrum simultaneously with the stellar spectrum and to efficiently scramble the starlight before sending it to the spectrograph. In terms of measurements, the observed radial velocity (V_{obs}) must be corrected for the instrumental drift (V_{inst} , mainly due to points 1 and 2 above) and for the Earth’s barycentric motion (V_{Earth} , point 3 above) to become the stellar barycentric radial velocity $V_{\text{star}} = V_{\text{obs}} - V_{\text{inst}} - V_{\text{Earth}}$ used in the Keplerian analysis described in Sect. 2.2. Two techniques have successfully been developed to accomplish this. If both these techniques use a cross-dispersed echelle

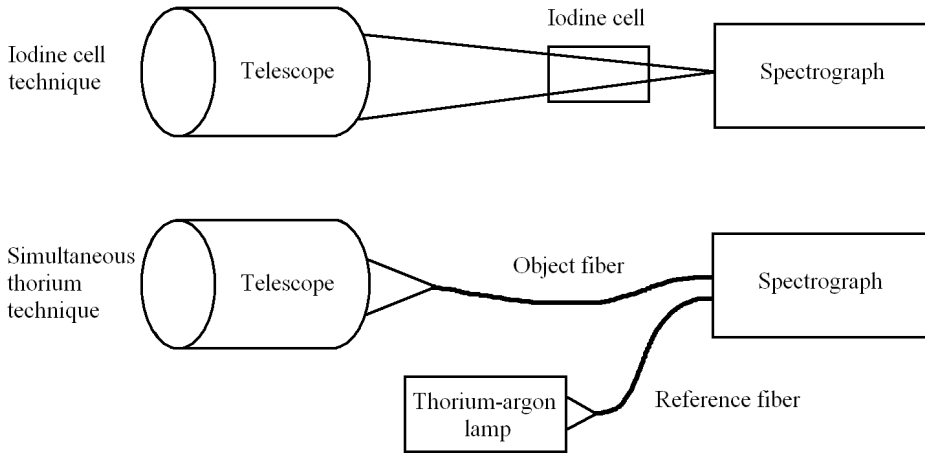


Fig. 3. Principle of the two techniques used to obtain high-precision radial velocities.

spectrograph and track instrumental drifts by means of a simultaneous wavelength calibration, they differ fundamentally in their approach and in their design.

2.3.2 The simultaneous reference technique

As illustrated on Fig. 3 (lower panel), the simultaneous reference technique involves the use of two optical fibers to feed the spectrograph: the so-called object fiber which records the starlight, and the so-called reference fiber which records the light from a wavelength reference source. In practice, the two fibers are brought into the entrance plane of the spectrograph in close proximity to one another, separated in the direction perpendicular to the main dispersion. The object and the reference spectra are then recorded simultaneously, the two sets of echelle orders being distinct and alternate on the detector. The simultaneous reference technique was pioneered on the ELODIE spectrograph (Baranne et al. 1996), and up to now all the spectrographs based on this technique have used as reference source a thorium-argon (ThAr) lamp. The method is thus commonly known as the simultaneous thorium technique.

A distinguishing feature of the simultaneous reference technique is that it can achieve high radial-velocity precision only if implemented on fiber-fed spectrographs with high mechanical and thermal stability. The use of optical fibers equipped with a scrambling device is indeed essential to reduce instabilities in illumination and variations of instrumental profile, both of which cannot be corrected by the simultaneous calibration. As to the thermal stabilization, it is meant to keep the optical paths of the two beams very similar within the spectrograph. Under such circumstances, the residual instrumental drifts experienced by the two beams are highly correlated and the velocity drift measured by the reference channel can be used to correct the object channel.

If the simultaneous thorium technique puts considerable demands on the instrumentation, the Doppler analysis is relatively straightforward. Radial velocities are traditionally obtained by numerically cross-correlating the observed spectra with box-shaped, binary (0 and 1 values) templates called masks (Baranne et al. 1996; Pepe et al. 2002a). Schematically, the cross-correlation function (CCF) is constructed by shifting the velocity of the mask by increasing amounts over a window roughly centered on the radial velocity of the star (Fig. 4). The better the alignment between the stellar lines and their box-shaped counterparts in the mask, the lower the cross-correlation value. The CCF is thus minimal when the velocity of the mask perfectly matches the radial velocity of the star (middle panel in Fig. 4). For slowly rotating dwarfs ($v \sin i \lesssim 10 \text{ km s}^{-1}$), the central part of the CCF is well approximated by a Gaussian function and the radial velocity of the star is measured by the center of the best-fit Gaussian. Note that radial velocities obtained through cross-correlation are free from most of the systematic errors listed in Sect. 2.3.1 only relative to the stellar mask, which defines the velocity zero point.

The masks used for cross-correlation are of two types: stellar and thorium. Stellar spectra are cross-correlated with stellar masks whose nonzero zones corresponds to the theoretical positions and widths of stellar absorption lines at zero velocity. Experience shows that there is no need to use a different mask for each star. Common practice is to use a few masks corresponding to the main spectral subtypes (e.g. G2, K5, and M2). Stellar masks are built either from high-resolution, high signal-to-noise observed spectra or from synthetic spectra. Reference thorium spectra are cross-correlated with a thorium mask built from the atlas of Palmer & Engleman (1983) and from the updated line list of Lovis & Pepe (2007).

Stabilized spectrographs searching for planets using the simultaneous thorium technique include ELODIE (1.93-m Telescope, Haute-Provence, France; dismounted in 2006), CORALIE (Leonard Euler Telescope, La Silla, Chile), HARPS (3.6-m ESO Telescope, La Silla, Chile), and SOPHIE (1.93-m Telescope, Haute-Provence, France). The radial-velocity precision has considerably improved from ELODIE to HARPS and is now better than 1 m s^{-1} (Sect. 4.3).

2.3.3 The gas cell technique

The basic feature of the gas cell technique is to pass the starlight through a cell containing an absorbing medium (the reference source) before entry into the spectrograph (Fig. 3, upper panel). In this way, absorption lines from the reference source superimpose on the stellar spectrum, providing a fiducial wavelength scale that experiences the same instrumental shifts and distortions as the stellar spectrum. Since the gas cell is at rest relative to the observatory, spurious instrumental shifts are measured by the wavelength shift of the reference lines. The reference spectrum also provides a specification of the instrumental profile (IP) at each position on the detector, allowing for the measurement and correction of IP variations. The first application of the gas cell technique to planet

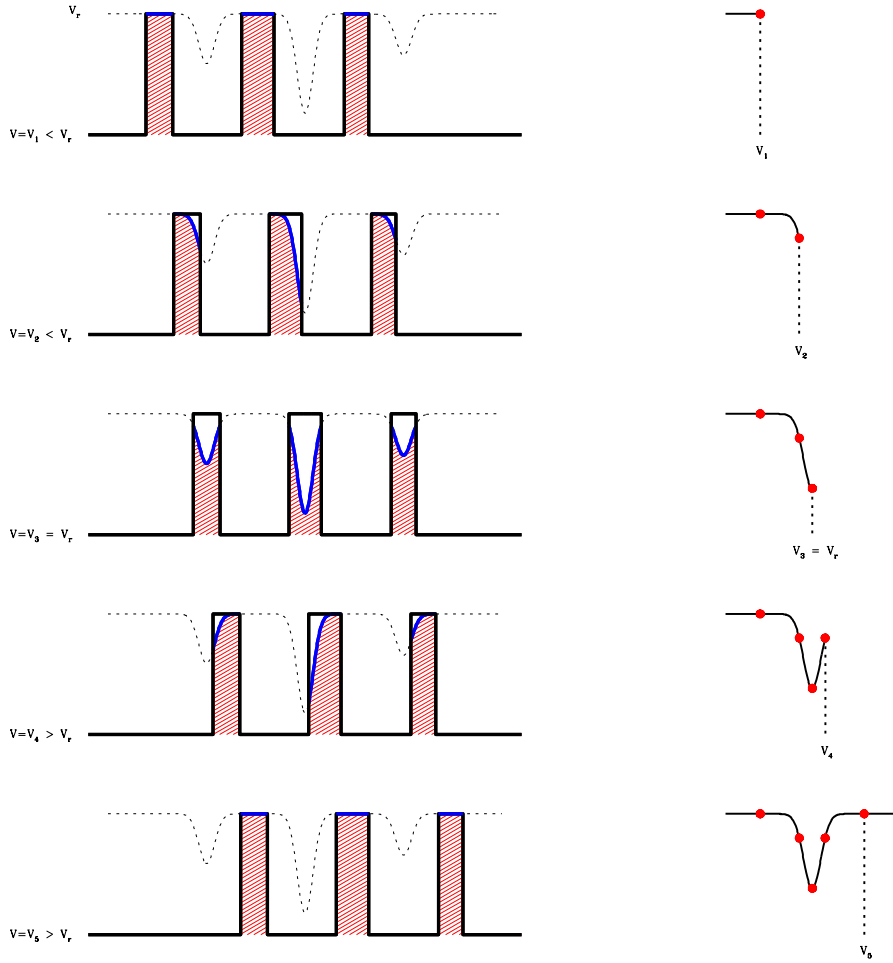


Fig. 4. Illustration of the construction of the cross-correlation function. Diagrams on the left represent the stellar spectrum (dashed lines) and the binary mask (solid lines, transmission zones depicted as hatched areas). Diagrams on the right show the result of the cross-correlation process. Courtesy of Claudio Melo.

searches was made by Campbell et al. (1988), who used a hydrogen fluoride (HF) cell (Campbell & Walker 1979). At present, all planet search programs based on this technique use an iodine cell and the technique is commonly referred to as the iodine cell technique.

Instrumentally, the iodine cell technique is easily implemented on any existing slit spectrograph. The main complication of the method resides in the Doppler analysis. In practice, spectra taken through the iodine cell are broken up into

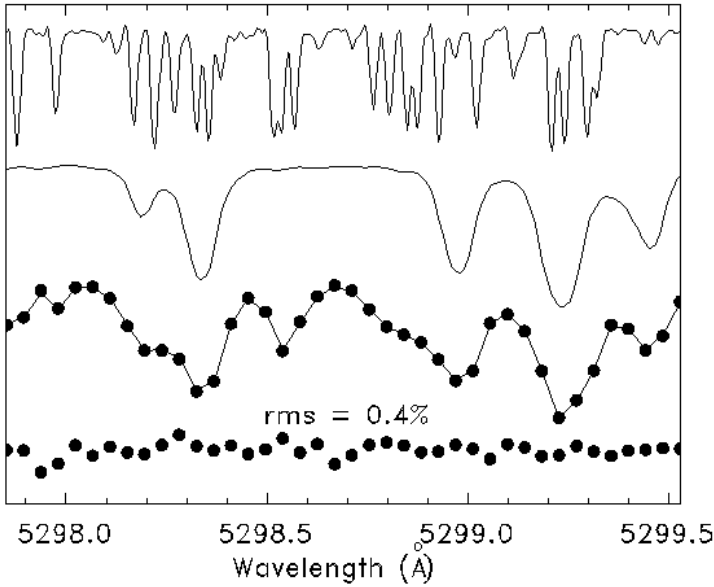


Fig. 5. Illustration of the modeling process for the iodine cell technique. Top: transmission function of the iodine cell (T_{I_2}) as measured by the FTS. Second: a template stellar spectrum (proxy for I_s). Third: the composite spectrum of the same star, as observed through the cell (dots) and as modeled (solid line). Bottom: ten times the difference between the model and the observations. Figure from Butler et al. (1996).

several hundred “chunks” of length $\sim 2 \text{ \AA}$. On each chunk the composite spectrum is modeled as

$$I_{obs}(\lambda) = k [T_{I_2}(\lambda)I_s(\lambda + \Delta\lambda)] * IP \quad (2.8)$$

where I_s is the intrinsic stellar spectrum, T_{I_2} is the transmission function of the iodine cell, IP is the in situ instantaneous instrumental profile, and the constant k is a normalization factor. The wavelength shift, $\Delta\lambda$, is the topocentric Doppler shift of the star. The barycentric radial velocity is obtained by correcting this topocentric Doppler shift for the Earth’s barycentric motion and by converting the result into a radial velocity using an elaborated version of the Doppler formula. Again, the barycentric radial velocity obtained in this way is not an absolute velocity; it is precise only relative to a stellar template, which defines an arbitrary velocity zero point.

As shown by Eq. 2.8, the modeling process requires two input functions, I_s and T_{I_2} , plus the knowledge of the instrumental profile. The transmission function of the cell is measured directly by obtaining a spectrum of the cell with a Fourier-Transform Spectrometer (FTS). The intrinsic stellar spectrum is more difficult to obtain since it cannot be measured directly. I_s is usually generated by taking a

high signal-to-noise spectrum of the program star without the iodine cell in place (which gives $I_s * IP$) and by deconvolving this spectrum from the instrumental profile. The instrumental profile cannot be measured directly either. It is commonly generated by comparing observations of a hot, rapidly rotating star (which basically gives $T_{I_2} * IP$) with the reference FTS iodine spectrum.

The whole modeling process is illustrated on Fig. 5 and typically requires 13 parameters: 2 for the wavelength scale, 1 for the topocentric Doppler shift of the star, and 10 for the description of the instrumental profile. These parameters are determined by comparing a series of models to the observed spectrum through a least-squares fit. We refer the reader to Marcy & Butler (1992), Valenti et al. (1995), and Butler et al. (1996) for complementary information on the practical aspects of the iodine cell technique.

Echelle spectrographs equipped with an iodine cell and actively used for planet searches include HAMILTON (Shane/CAT, Lick, USA), HIRES (KECK, Mauna Kea, USA), UCLES (AAT, Siding Spring, Australia), HRS (HET, Davis Mountains, USA), and UVES (VLT, Paranal, Chile). The iodine cell technique has long demonstrated a precision of 3 ms^{-1} (Butler et al. 1996), but the precision seems to have not much improved since then. Residuals around the best planetary orbits published so far indicate a precision of $\sim 2.5 \text{ ms}^{-1}$ (Butler et al. 2006; Fischer et al. 2006; Wright et al. 2008).

2.4 Limitations on Doppler spectroscopy

Limitations on Doppler measurements can be classified into three broad categories: photon count, technical, and astrophysical. We describe here photon count and astrophysical limitations. Technical limitations related to the simultaneous thorium technique will be discussed in Sect. 4.3.

2.4.1 Photon count limitations

The ultimate limit to the attainable Doppler precision is that set by photon-counting statistics. As proposed by Connes (1985), the uncertainty related to photon noise can be quantified by a quality factor, Q , which is a sole function of the line profile in the case of pure photon noise. For spectral types between F2V and K7V, Q increases towards the blue and Q is the highest for a K5V star (Bouchy et al. 2001). These two trends reflect the evolution in the strength and width of metal lines along the spectral sequence (late-type stars have more “peaky” lines) and the fact that these lines are more numerous between 4000 and 4500 Å than between 6000 and 6800 Å. Q is also sensitive to rotational line broadening, decreasing as $1/v \sin i$ for $v \sin i > 6 \text{ km s}^{-1}$. For these reasons, early-type stars (\lesssim F6) with few and broad absorption lines do not permit high-precision Doppler measurements, whereas slowly rotating K dwarfs are ideally suited for high-precision Doppler programs.

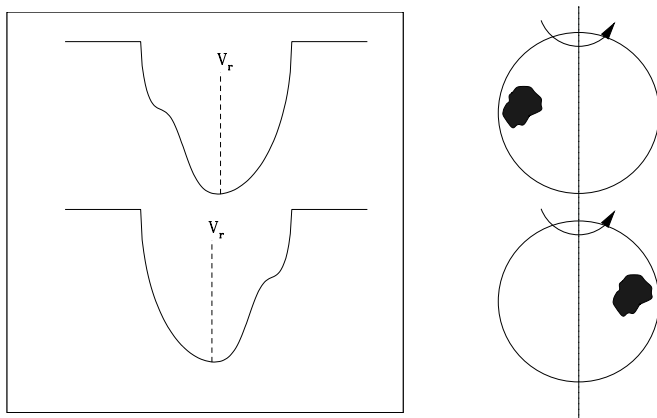


Fig. 6. Illustration of the effect of a starspot on the profile of the cross-correlation function and on the determination of its centroid (radial velocity). The effect has been exaggerated for illustrating purposes.

2.4.2 Astrophysical limitations

Stellar activity Magnetic phenomena at the surface of solar-type stars induce radial-velocity variations through the temporal and spatial evolution of spots, plages, and convective inhomogeneities (Saar & Donahue 1997; Saar et al. 1998). Figure 6 illustrates how the rotation of a starspot modifies the line profiles – and equivalently the CCF profile – affecting the determination of the radial velocity. When the starspot pattern is long-lived, variations in line asymmetry are modulated by the rotational period of the star and can mimic a planetary signal (e.g. Queloz et al. 2001; Bonfils et al. 2007). When the star is observed longer than the typical lifetime of starspots, the signal becomes incoherent and is detected as radial-velocity “noise”. Although less confusing, this is still annoying since it may inhibit the detection of planetary signals of lower amplitude.

In practice, radial-velocity perturbations related to stellar activity are referred to as “stellar jitter”. Stellar jitter depends on effective temperature, stellar activity, and projected rotational velocity (Saar et al. 1998; Santos et al. 2000b; Wright 2005), but these dependencies cannot be modeled in detail yet. Typical values of stellar jitter are $\lesssim 5 \text{ m s}^{-1}$ for slowly rotating, chromospherically quiet G-K dwarfs (Santos et al. 2000b; Wright 2005) and $\lesssim 50 \text{ m s}^{-1}$ for F5-M2 young, active dwarfs (Paulson et al. 2004). The above values explain why high-precision Doppler planet searches select their targets among old, slowly rotating inactive stars.

To quantify the activity level of their (potential) targets, Doppler planet searches traditionally use the parameter R'_{HK} , which represents the fraction of a star’s bolometric flux emitted by the chromosphere in the Ca II H and K lines (Noyes et al. 1984). Since this chromospheric emission is closely related to the surface magnetic flux, a high R'_{HK} value is an indication that a star may exhibit significant activity-

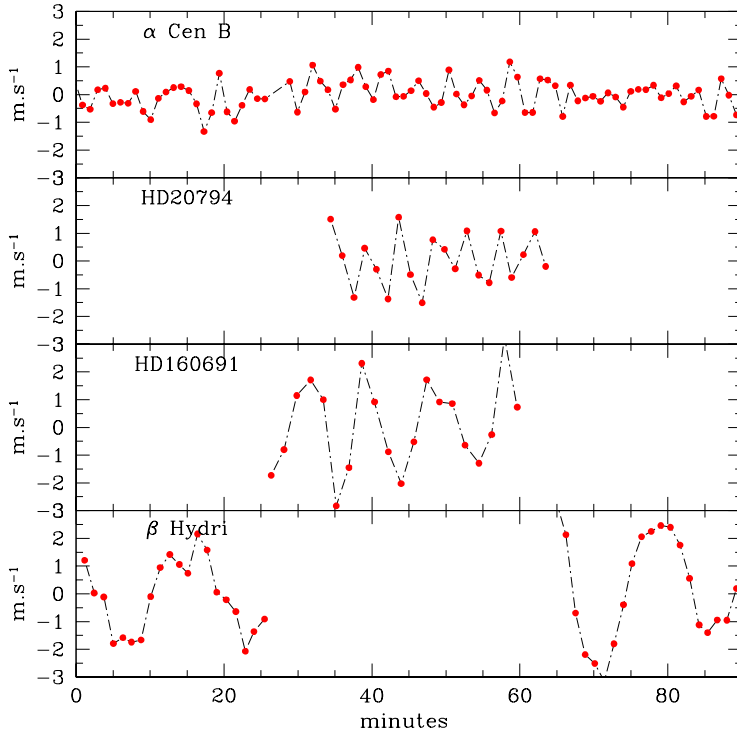


Fig. 7. Sequences of HARPS radial-velocity measurements on four solar-type stars. Solar-like oscillations are clearly visible on each of these sequences.

related velocity variations. But a high R'_{HK} index does not prove that a given Doppler signal is of stellar origin. To prove this, one can search for a periodic modulation in the Ca II flux, in the bisector of the cross-correlation function, or in photometric observations (e.g. Queloz et al. 2001; Desort et al. 2007; Bonfils et al. 2007). These diagnostics are pretty effective at identifying activity-related velocity variations in G, K, and M dwarfs.

Solar-like oscillations The Sun oscillates in many low-amplitude modes simultaneously, each mode being characterized by a maximum amplitude $\lesssim 20 \text{ cm s}^{-1}$ and a period between 3 and 15 minutes. This so-called five-minute oscillation is excited stochastically by turbulent convective motions near the solar surface. Main-sequence stars with significant outer convection zones should all exhibit similar pulsations, called solar-like oscillations in this more general context. Recent observations have shown that this is indeed the case (Fig. 7). It should be emphasized that while individual modes have typical amplitudes in the range $10\text{-}50 \text{ cm s}^{-1}$ for main-sequence stars, their interference can produce radial-velocity variations up to about 10 times these values on time scales of minutes. Although these oscilla-

tions constitute a very interesting tool to probe the structure of stellar interiors (this is asteroseismology; see the contribution by Vauclair), they are essentially “an annoying source of noise” when viewed from the side of very high precision planet searches. As explained in Sect. 4.3, an adequate observing strategy allows fortunately to largely average out this noise, reducing its impact on the search for low-mass planets.

Contamination effects Slit spectrographs used for planet searches have typical on-sky slit widths of 0.5-1", while fiber spectrographs have typical on-sky fiber diameters of 1-3". The light from an object close to the scientific target may thus also fall within the slit/fiber, contaminating the target's spectrum and altering the determination of the target's velocity. For this reason, known binary stars closer than 2-6" are generally rejected from Doppler planet search programs (see Eggenberger & Udry 2007 for details). Yet, some close star systems are present in the samples of large-scale Doppler surveys and it may happen that a star turns out to be a binary, or that a presumed binary system turns out to be triple. The latter case is of particular concern because unrecognized triple systems may under some circumstances mimic the radial-velocity signature of a planetary companion to a single star (e.g. Santos et al. 2002; Zucker et al. 2003). Unrecognized triple systems can be identified indirectly through bisector analyses (e.g. Santos et al. 2002; Eggenberger et al. 2003) and directly using two-dimensional correlation (e.g. Zucker et al. 2003; Eggenberger & Udry 2007). Due to the strong bias against (moderately) close binaries in the samples of regular Doppler planet searches, contamination effects remain marginal and do not significantly affect planet searches.

3 Statistical properties of planetary systems with giant planets

The number of planetary companions detected through Doppler spectroscopy has increased exponentially since 1995, yielding an abundant observational material to characterize the properties of giant planets orbiting within 3 AU from their host stars. These data have been used extensively to study the distributions of planet properties and to quantify the incidence of giant planets among different populations of stars (e.g. Marcy et al. 2005a; Udry et al. 2007; Udry & Santos 2007). As these statistical features are thought to bear fossil imprints of planet formation and evolution processes, they provide a crucial link between observation and theory. This link has recently been strengthened by the new ability of core accretion models to generate synthetic planet populations, which can be compared with the observed sample of extrasolar planets (Ida & Lin 2004a; Alibert et al. 2005; Mordasini et al. 2009, in prep.).

3.1 Doppler surveys and their samples

Radial-velocity planet search programs have traditionally selected their targets to optimize the achievable Doppler precision, favoring bright, chromospherically inactive main-sequence stars with spectral types between \sim F8 and \sim M0. Among

these “classical” programs, those which have most significantly contributed to the present discoveries are: the ELODIE Planet Search (~ 330 G-K dwarfs; Perrier et al. 2003), the California and Carnegie Planet Search (~ 1100 F-G-K-M dwarfs; Marcy et al. 2005b), the CORALIE Planet Search (~ 1650 G-K dwarfs; Udry et al. 2000), the Anglo Australian Planet Search (~ 230 F-G-K-M stars; Tinney et al. 2005), and the HARPS Planet Search (~ 1500 G-K-M dwarfs; Mayor et al. 2003). To this list we can add the so-called “metallicity-biased” surveys, N2K (~ 2000 F-G-K dwarfs; Fischer et al. 2005) and ELODIE² (~ 1200 G-K dwarfs; da Silva et al. 2006), which aim at detecting short-period giant planets orbiting metal-rich stars. Omitting the metallicity-biased surveys, these programs collectively monitor about 3000 F-G-K dwarfs of the solar neighborhood.

Planet searches targeting M dwarfs were originally limited by the faintness of their targets (Delfosse et al. 1998; Marcy & Butler 1998). Recent instrumental developments coupled with the use of larger telescopes have considerably improved the situation, allowing the inclusion of a significant number of M dwarfs in the present surveys (Endl et al. 2003; Butler et al. 2004; Bonfils et al. 2005; Bouchy et al. 2007). In total, about 300 nearby M dwarfs are now being monitored.

As explained in Sect. 2.4, main-sequence stars earlier than $\sim F6$ are not suited for high-precision Doppler measurements and classical surveys avoid them accordingly. A recent attempt has been made to extract precise radial velocities for A and F dwarfs following a dedicated approach (Galland et al. 2005), but even with this method planet searches remain limited by stellar activity. An alternative approach to study planet occurrence among stars more massive than the Sun consists in observing these stars when they have evolved off the main-sequence, becoming G-K giants or subgiants. Doppler planet searches around G-K (sub)giants have gradually expanded during the past five years and some hundred stars are now regularly observed (Frink et al. 2002; Setiawan et al. 2003; Hatzes et al. 2005; Johnson et al. 2006; Lovis & Mayor 2007; Niedzielski et al. 2007; Sato et al. 2005).

A notable built-in bias affecting classical Doppler planet searches is the avoidance of binaries closer than $2\text{-}6''$ (Sect. 2.4.2). Due to this discrimination, current data only provide sparse information on the suitability of $\lesssim 200$ AU binaries for planetary systems. But again the situation is improving, and radial-velocity planet searches have recently been extended to spectroscopic and moderately close visual binaries (e.g. Eggenberger & Udry 2007; Mutterspaugh et al. 2007).

Turning to statistical studies, it should be noted that rigorous analyses including the calculation of detection thresholds and survey completeness are available only for the oldest programs (Cumming et al. 1999; Endl et al. 2002; Naef et al. 2005; Wittenmyer et al. 2006; Cumming et al. 2008), and with the exception of Cumming et al. (2008) these analyses contain too few planet detections to study the distributions of planet properties. Therefore, even though they have not been rigorously corrected for selection effects yet, the two surveys best suited for sta-

²Now replaced by a SOPHIE program (Bouchy et al. 2007).

tistical analyses are the CORALIE survey with its HARPS extension and the combined Lick+Keck+AAT survey.

3.2 Occurrence rate of giant planets

At present, true occurrence rates are available for the ELODIE and for the Keck programs. Results from the ELODIE survey indicate that the fraction of stars with a planet more massive than $0.5 M_{\text{Jup}}$ is $0.7 \pm 0.5\%$ for $P < 5$ days ($a \lesssim 0.06$ AU) and $7.3 \pm 1.5\%$ for $P < 3900$ days ($a \lesssim 4.8$ AU) (Naef et al. 2005). For the same mass and period ranges, the Keck survey obtains $0.65 \pm 0.40\%$ and $8.6 \pm 1.3\%$ (Cumming et al. 2008).

It should be emphasized that according to planet formation models, giant planets reside preferentially beyond ~ 3 AU, while the overall planet population is dominated (in number) by low-mass planets (Ida & Lin 2004a; Mordasini et al. 2007). Taking into account the selection effects inherent to Doppler spectroscopy, the ELODIE and Keck programs could detect only a small fraction of the overall planet population ($\sim 6\%$ according to Mordasini et al. 2007). The above figures thus lend support to the hypothesis that planets are common around solar-type stars.

3.3 Mass, period, and eccentricity distributions

3.3.1 Mass distribution

As explained in Sect. 2.2, Doppler spectroscopy does not yield the true mass of planetary companions but only the product $m_p \sin i$, which is a lower limit on the planet mass. Nonetheless, as shown by Jorissen et al. (2001), the distribution of minimum masses is a good proxy for the mass distribution³.

The distribution of minimum masses is shown in Fig. 8. While most of the detected planets have minimum masses below $5 M_{\text{Jup}}$, the distribution exhibits a long tail towards minimum masses larger than $10 M_{\text{Jup}}$. For orbital periods less than a decade, there is a scarcity of companions with (minimum) masses between ~ 10 and $\sim 100 M_{\text{Jup}}$ (e.g. Zucker & Mazeh 2001). This gap in the mass distribution – called the brown dwarf desert – constitutes the most obvious evidence that extrasolar planets and stellar companions belong to two distinct populations which formed through two different mechanisms. The two populations are not completely disconnected, however, as some overlap seems to exist between ~ 10 and $\sim 20 M_{\text{Jup}}$. Distinguishing massive planets from low-mass brown dwarfs on the sole basis of their (minimum) mass may thus be hazardous, preventing at present a determination of the upper limit to the mass of a planet.

The low-mass side of the minimum mass distribution is strongly affected by selection effects below the mass of Saturn ($0.3 M_{\text{Jup}}$), but despite this incomplete-

³For the sake of conciseness, we often use the terms “mass” and “mass distribution” instead of “minimum mass” and “minimum mass distribution”. However, we make the difference or use the additional term “true mass” when the difference is important.

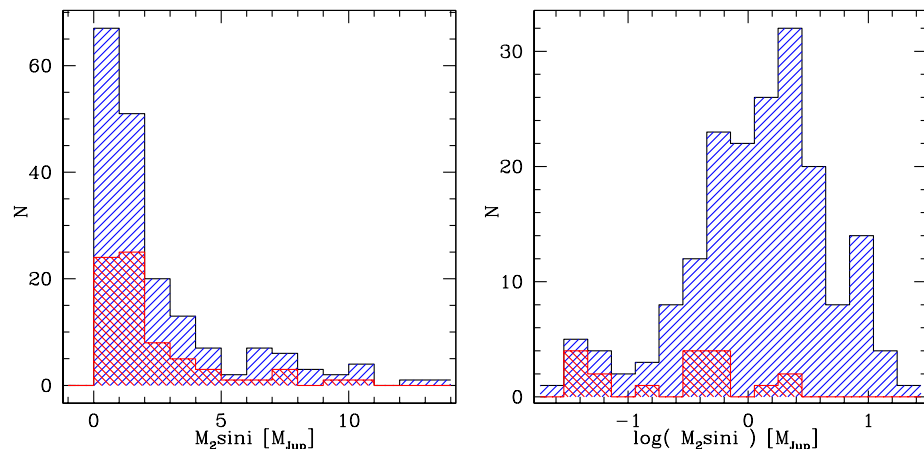


Fig. 8. Distribution of planet minimum masses in linear (*left*) and logarithmic (*right*) scales. The double-hatched histogram represents the planets detected with CORALIE (*left*) or with HARPS (*right*).

ness the distribution seems to turn upwards near $0.1 M_{\text{Jup}}$. This low-mass part of the distribution will be discussed in Sect. 4.2.2.

3.3.2 Period distribution

The period distribution is shown in Fig. 9. At short periods, there is a pile-up of planets with periods between 2 and 5 days. These are the so-called hot Jupiters like 51 Peg b. The detection of Jovian planets orbiting their stars in just a few days has been a major surprise since prior to this discovery theory predicted that giant planets would form – and by implication exist – only beyond a few AU. Although not completely excluded, forming these planets in situ is difficult (Bodenheimer et al. 2000) and the first detections of hot Jupiters have posed a serious challenge to planet formation theories. According to the revised models, short-period giant planets likely formed beyond a few AU and then migrated inwards as a result of their tidal interaction with the gaseous disk (e.g. Lin et al. 1996; Ida & Lin 2004a; Mordasini et al. 2007; Armitage 2007). The discovery of close-in giant planets like 51 Peg b has thus revived the notion of planetary migration (see the contributions by Terquem and Ida) and there is now little doubt that many extrasolar planets have formed at locations which do not correspond to those where they are observed today.

The origin and even the existence of the pile-up of planetary companions with periods close to 3 days are still being debated. If hot Jupiters have undergone extensive migration within a gaseous disk, there is a priori little reason why they should have stopped at small radii rather than plunge into their star. Some mechanisms have thus been proposed to stop orbital migration and to park gi-

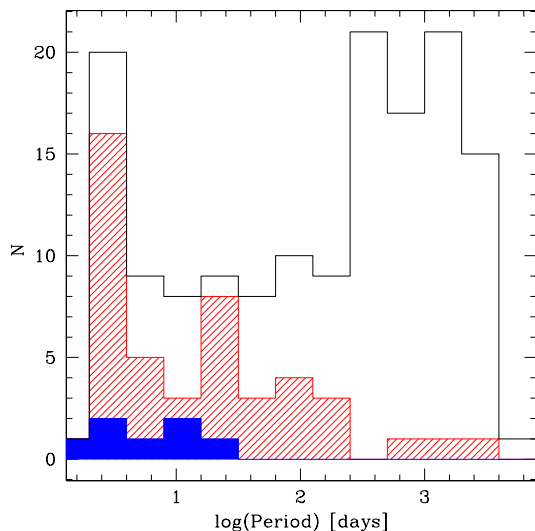


Fig. 9. Period distribution for extrasolar planets. The hatched histogram represents light planets with $m_p \sin i \leq 0.75 M_{\text{Jup}}$, while the filled histogram represents Neptune-mass planets with $m_p \sin i \leq 21 M_{\oplus}$.

ant planets on close orbits: the existence of a central cavity in the disk (e.g. Lin et al. 1996; Kuchner & Lecar 2002), tidal interactions with the spinning host star (e.g. Trilling et al. 1998; Pätzold & Rauer 2002), or Roche lobe overflow (e.g. Trilling et al. 1998; Gu et al. 2003). Alternative scenarios for the formation of hot Jupiters involve resonant interactions with a disk of planetesimals (Murray et al. 1998), or tidal circularization of highly eccentric orbits (e.g. Ford & Rasio 2007; Fabrycky & Tremaine 2007).

At longer periods, the number of planets remains fairly constant between ~ 7 and ~ 250 days, and then increases abruptly. The time baseline of ongoing programs is still too short to tell whether the period distribution (in logarithmic scale) remains flat from ~ 300 days to ~ 4 years, or increases continuously beyond ~ 250 days. In either case, current data indicate that there exists a large reservoir of giant planets with periods above 5 years ($a \gtrsim 3$ AU) which we are just beginning to detect. This shows that the main limitation at the moment for the detection of analogs of our Solar System is not the Doppler precision but the duration of the surveys.

3.3.3 Period-eccentricity diagram

Figure 10 shows the period-eccentricity diagram for both extrasolar planets and stellar binaries with solar-type primaries. This plot makes it clear that most of the extrasolar planets have anomalous eccentricities compared with those of

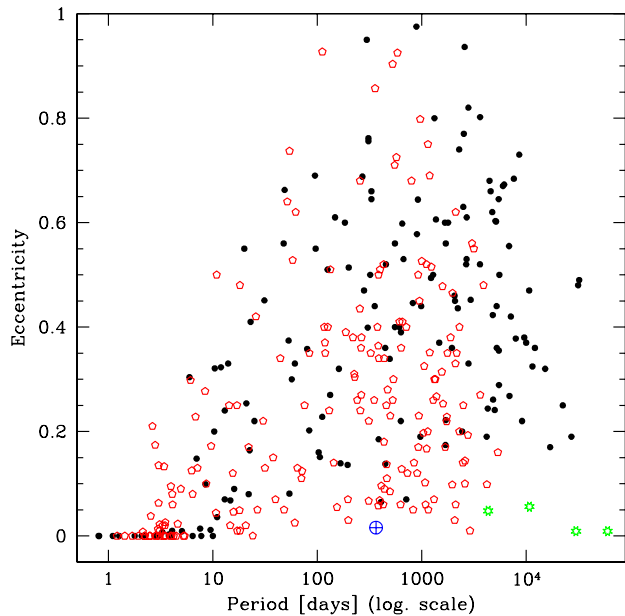


Fig. 10. Period-eccentricity diagram for extrasolar planets (open pentagons) and for stellar companions to solar-type stars (black dots). The Earth and the four giant planets of the Solar System are also indicated (Earth and starry symbols at the bottom).

Jupiter and Saturn (0.048 and 0.056, respectively). Planets with periods below ~ 5 days tend to have small eccentricities due to tidal dissipation (e.g. Rasio et al. 1996). Tidal circularization becomes ineffective at longer periods and planetary eccentricities then span almost all the allowable range with a median value of 0.29.

These high planetary eccentricities are very puzzling since formation in a disk is thought to yield almost circular orbits. If it is so indeed, some additional processes must drive the planets out of their initially circular orbits. Numerous mechanisms have been proposed to excite planetary eccentricities (see Ford & Rasio 2007 for a review and references), including strong gravitational scattering between planets, secular interactions with a distant companion in a highly inclined orbit, or interactions of orbital migration with mean motion resonances (see also Sect. 3.4). While these three mechanisms are all supported by some observational evidence, none can reproduce the overall eccentricity distribution. It is thus likely that several mechanisms contribute in determining the eccentricity distribution.

Contrary to the mass distribution, the eccentricity distribution of extrasolar planets is not radically different from that of stellar companions to solar-type stars, though small differences exist (e.g. Halbwachs et al. 2005). This observation has sometimes been considered as an indication that extrasolar planets and stellar companions belong to the same population and share a common origin

(Stepinski & Black 2000). Actually, it is more probable that the formation mechanisms were distinct, but that the orbital eccentricities were excited through similar mechanisms.

3.4 Multiple planet systems

Among the 253 planet-host stars with Doppler measurements, 30 are orbited by multiple planets, the most prolific systems being presently 55 Cnc with 5 planets (Fischer et al. 2008) and μ Ara with 4 planets (Pepe et al. 2007). The observed fraction of multiple planet systems is 12%, meaning that the probability of finding a second planet is enhanced by a factor of about two with respect to the probability of finding the first planet. This multiplicity rate is certainly a lower limit as multiple planet systems require more Doppler observations spanning a longer time baseline to extract the different Keplerian signals. In the surveys with the longest duration the fraction of multiple systems ranges from 25% to 50% (Fischer & Valenti 2005; Udry & Santos 2007; Wright et al. 2007). These results suggest that like the Sun, most solar-type stars are orbited by systems of planets.

The presence of two (or several) planets interacting one with another is interesting because it increases our potential ability to characterize the system's orbital configuration and formation history. For instance, strong mutual interactions between two planets allow to (partially) remove the $\sin i$ degeneracy, yielding true planetary masses (e.g. Chiang et al. 2001; Rivera et al. 2005). From a more specific point of view, the existence of pairs of planets locked in low-order mean motion resonances (i.e. with commensurable periods such as GJ 876 b and c) indicates that some planets experienced smooth convergent migration (e.g. Lee 2004; Kley et al. 2005). Alternatively, the current orbital configuration of the three giant planets orbiting Ups And suggests that planet-planet scattering occurred in this system (Ford et al. 2005).

3.5 Properties of the host stars

Planet formation being a by-product of star formation, some stellar characteristics may provide important information about the conditions leading to planet formation. Recent work has shown that the occurrence rate and the properties of giant planets depend on the mass, metallicity, and multiplicity status of the parent star.

3.5.1 Stellar metallicity

Not long after the discovery of the first extrasolar planets, it was noticed that planet-bearing stars were systematically metal-rich compared to the Sun (e.g. Gonzalez 1997; Santos et al. 2000a). Recent studies have shown that planet occurrence is a rising function of the parent star metallicity (Fig. 11). Specifically, $\sim 25\%$ of the stars with twice the metal content of the Sun ($[\text{Fe}/\text{H}] = 0.3$) harbor a giant planet, against only $\sim 3\%$ for solar-metallicity stars (Santos et al. 2004b; Fischer & Valenti 2005). This observation has motivated the metallicity-biased surveys mentioned in Sect. 3.1.

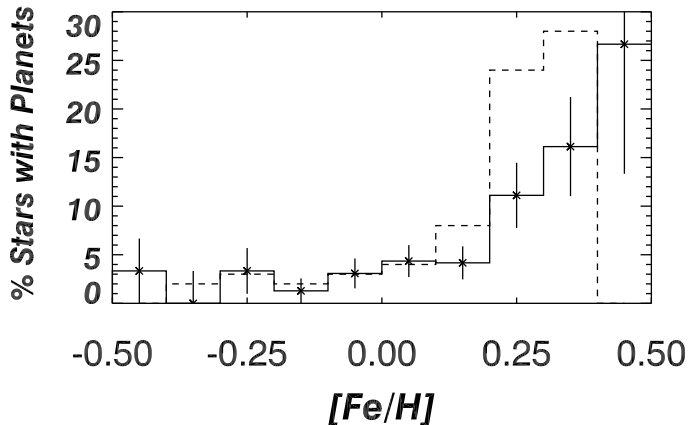


Fig. 11. Percentage of planet-host stars as a function of stellar metallicity. The dashed line shows the results from Santos et al. (2004b) and the solid line shows the results from Fischer & Valenti (2005).

Three explanations have been proposed to understand this correlation: (1) an enhanced metallicity in the protoplanetary disk could be more conducive to planet formation, (2) the infall of metal-rich planetary material onto the host stars could have enriched their outer layers, or (3) there might be an “orbital period bias” due to the dependence of migration rates on metallicity (Livio & Pringle 2003) or to the inward shift of the optimum region for giant planet formation in metal-poor stars (Pinotti et al. 2005). Some observational evidence for the last two hypotheses have been reported in the literature (e.g. Israelian et al. 2001; Sozzetti 2004), but most analyses suggest that the overall metallicity excess observed in planet-host stars has a primordial origin and reflects the high metallicity in the protoplanetary disk (e.g. Pinsonneault et al. 2001; Livio & Pringle 2003; Santos et al. 2003; Fischer & Valenti 2005). This conclusion is corroborated by core accretion models, which reproduce the observed correlation (Ida & Lin 2004b; Benz et al. 2006). Disk instability being apparently insensitive to metallicity (Boss 2002), the metal-rich nature of planet-host stars is commonly considered as a major evidence that most of the giant planets we observe today formed through core accretion.

3.5.2 Stellar mass

The occurrence rate of Jovian planets appears to correlate with stellar mass, giant planets being rarer around M dwarfs (Endl et al. 2006; Butler et al. 2006; Bonfils et al. 2007) and more frequent around intermediate-mass stars (Lovis & Mayor

2007; Johnson et al. 2007). Another quantity which correlates with stellar mass is the “average mass of planetary systems” as defined by Lovis & Mayor (2007). This second trend may simply be a consequence of the first correlation, but it could also indicate that planetary systems tend to be more massive around more massive stars. Under the assumption that the mass of protoplanetary disks scales with stellar mass – which remains to be confirmed – both trends are supported by the core accretion model (Laughlin et al. 2004; Ida & Lin 2005; Kennedy & Kenyon 2008; Benz et al. 2008).

Remarkably, G-K (sub)giants hosting giant planets seem to lack the strong metal-rich tendency seen in F-G-K dwarfs (e.g. Pasquini et al. 2007; Takeda et al. 2008). It is thus likely that both metallicity and stellar mass impact the occurrence and the properties of giant planets. Larger samples of planets orbiting low- and intermediate-mass stars will be needed to confirm this observation and to disentangle the two effects.

3.5.3 Stellar multiplicity

Contrary to some expectations and despite the strong bias against their detection, giant planets have been found in various types of binaries and triple systems, including spectroscopic binaries with projected separations of ~ 20 AU (e.g. Eggenberger et al. 2004; Raghavan et al. 2006; Desidera & Barbieri 2007). Interestingly, some of these planets seem to possess distinctive characteristics when compared to planets orbiting single stars: (1) the most massive short-period planets are all found in binaries (Udry et al. 2002; Zucker & Mazeh 2002; Eggenberger et al. 2004), (2) the minimum period for a significant eccentricity seems larger for planets in binaries (~ 40 days) than for planets around single stars (~ 5 days; Eggenberger et al. 2004), and (3) the four planets with an eccentricity larger than 0.8 all have a stellar or brown dwarf companion (Tamuz et al. 2008). These trends may indicate that migration and postformation evolution proceed differently in some types of binaries than around single stars, as suggested by some theoretical studies (Kley 2000; Wu & Murray 2003; Fabrycky & Tremaine 2007).

4 The road to Earth twins

One of the main drivers of extrasolar planet searches is to understand the origin and the degree of uniqueness of a life-bearing planet like the Earth. There are thus strong motivations to search for rocky planets orbiting within the habitable zones of their stars, that is within the circumstellar region where a terrestrial planet can hold liquid water on its surface (e.g. Kasting et al. 1993). According to theoretical models, such planets should be numerous (e.g. Ida & Lin 2004a; Mordasini et al. 2007). The main obstacle to their discovery through Doppler spectroscopy is their low mass, which translates into an extremely low-amplitude radial-velocity signal (9 cm s^{-1} for the Earth).

The detection of low-mass planets being closely related to the ultimate precision achieved by Doppler surveys, the first Neptune-mass planets ($10 M_{\oplus} < m_p \sin i \leq$

$25 M_{\oplus}$) were found only four years ago (Butler et al. 2004; McArthur et al. 2004; Santos et al. 2004a). The first observation of a so-called super-Earth ($2 M_{\oplus} \leq m_p \sin i \leq 10 M_{\oplus}$) was announced one year later (Rivera et al. 2005) and opened the way to a series of discoveries. This new step forward in planet searches was made possible first by the development of a new generation of very precise instruments whose prototype is the HARPS spectrograph, and second by the application of a careful observing strategy to improve detection capabilities and minimize the impact of stellar noise.

4.1 HARPS, a new-generation instrument to search for low-mass planets

In 1998 the European Southern Observatory (ESO) issued an announcement of opportunity for the procurement of an instrument dedicated to the search for extrasolar planet at the unequaled precision of 1 m s^{-1} . This led to the development of the HARPS spectrograph, which was manufactured by the HARPS Consortium⁴. HARPS is mounted on the ESO 3.6-m telescope at La Silla Observatory (Chile) and it has been available to the astronomical community since October 2003

HARPS (High Accuracy Radial velocity Planet Searcher) is a fiber-fed, cross-dispersed echelle spectrograph covering the spectral range from 380 to 690 nm with a resolution $R = 115,000$ (Pepe et al. 2002b; Mayor et al. 2003; Rupprecht et al. 2004). Like its two predecessors, ELODIE (Baranne et al. 1996) and CORALIE (Queloz et al. 2000), HARPS uses the simultaneous thorium technique. But unlike its two predecessors, HARPS is placed inside a vacuum vessel, the operating pressure being kept below 0.01 mbar. The vacuum vessel is in turn located in a thermally stabilized enclosure and this two-stage insulation ensures a short-term (1 night) temperature stability of a few millidegrees. Thanks to this high environmental stability, instrumental drifts never exceed 1 m s^{-1} during the night, making HARPS the most stable spectrograph in the world.

In exchange for the delivery of the instrument to ESO, the HARPS Consortium received Guaranteed Time Observations (GTO; 500 observing nights over 5 years). Since July 2003, the consortium has used this time to carry out a comprehensive planet search program (Mayor et al. 2003). More than 60% of the GTO time is devoted to the search for low-mass planets around ~ 520 G-K-M dwarfs.

4.2 Observational results on low-mass planets

The present sample of low-mass planets (defined here as planets with $m_p \sin i \leq 25 M_{\oplus}$) comprises 18 objects (Mayor & Udry 2008 and references therein; Forveille et al. 2008). We present below some noteworthy detections made with HARPS in the context

⁴The HARPS Consortium is composed of the Geneva Observatory (leading institute), the Observatoire de Haute-Provence, ESO, the Physikalisches Institut der Universität Bern, and the Service d'Aéronomie du CNRS.

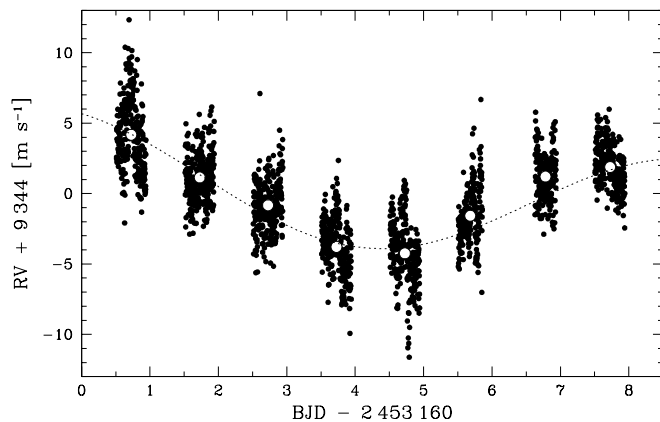


Fig. 12. Radial velocity measurements of μ Arae obtained during the asteroseismology campaign. White circles correspond to night averages. The dashed line shows the Keplerian orbit of the Neptune-mass planet confirmed by additional Doppler measurements. Figure from Bouchy et al. (2005a).

of the GTO program. We then discuss a few interesting statistical trends that are emerging among this new population of low-mass planets.

4.2.1 Noteworthy HARPS discoveries

A Neptune-mass planet around μ Arae The $10.5\text{-}M_{\oplus}$ planet around μ Arae (μ Arae c with a period of 9.6 days) was found serendipitously during an asteroseismology campaign (Santos et al. 2004a; Bouchy et al. 2005a). Prior to this detection, μ Arae was known to harbor a giant planet in a 743-day orbit (Butler et al. 2001) and a possible additional planetary companion in a wider orbit (Jones et al. 2002). The continuous monitoring of μ Arae within the HARPS GTO program led to the discovery of a fourth planet (Pepe et al. 2007), making this star host to a rich and complex planetary system.

As shown on Fig. 12, the amplitude of the radial-velocity signal of μ Arae c is similar to the peak-to-peak radial-velocity variation induced by solar-like oscillations. The detection of this tiny planetary signal thus strongly benefitted from the high measurement density of the asteroseismology campaign. Nonetheless, follow-up observations have shown that adopting an adequate observational strategy (Sect. 4.3), planets such as μ Arae c are within the detection capabilities of the HARPS GTO program.

The quasi-simultaneous discovery of Neptune-mass planets around 55 Cnc, GJ 436 and μ Arae raised the question of their origin and constitution. Are they sub- or near-critical planetary cores that failed to accrete large amounts of nebular gas (see Sect. 1), or are they the remnant of gaseous giant planets which lost a large fraction of their atmosphere through evaporation? While Santos et al. (2004a) favor an essentially rocky composition for μ Arae c, the gas giant remnant and the

ice-rock composition cannot be excluded (Baraffe et al. 2006; Brunini & Cionco 2005).

A trio of Neptunes around HD 69830 Two years ago, Lovis et al. (2006) reported the discovery of a planetary system made of three Neptune-mass objects (projected masses of 10.2, 11.8, and 18.1 M_{\oplus} ; periods of 8.7, 31.6, and 197 days) around HD 69830 (Fig. 13). This system possess two interesting characteristics: it is composed exclusively of low-mass planets, and it seems to harbor a massive asteroid belt within 1 AU (Beichman et al. 2005). According to Alibert et al. (2006), the innermost planet is essentially a rocky core, while the two outermost planets are rocky cores surrounded by a shell of fluid water and a gaseous envelope.

From the technical perspective, the values of the radial-velocity semiamplitudes (2.2, 2.7 and 3.5 ms^{-1}) make the three planetary signals undetectable with most of today's spectrographs. Considering only the most recent measurements made with an improved observing strategy, the root-mean-square (rms) of the residuals around the best-fit solution is 0.64 ms^{-1} and this value decreases to 0.35 ms^{-1} (bottom right panel of Fig. 13) when the observations are binned to yield one measurement per observing run (typical run duration of 10 days).

Two habitable super-Earths around Gl 581? The M4 dwarf Gl 581 also harbors a very interesting planetary system made of a hot Neptune ($m_p \sin i = 16 M_{\oplus}$, period of 5.4 days; Bonfils et al. 2005) and two super-Earths ($m_p \sin i = 5$ and 8 M_{\oplus} , periods of 13 and 83 days; Udry et al. 2007). These two super-Earths lie close to the inner and outer edges of the habitable zone of Gl 581, raising the question of their habitability. Models of planetary atmospheres indicate that planet c is probably too close to Gl 581 to be habitable (Selsis et al. 2007; von Bloh et al. 2007). Habitability prospects are much better for planet d, which may be an interesting target for future space missions aimed at searching for life signatures in the atmospheres of low-mass planets.

This system illustrates two advantages M dwarfs possess over solar-type stars: (1) the smaller mass of M dwarfs makes the detection of low-mass planets easier (Eq. 2.5), and (2) the habitable zone occurs farther in around M dwarfs than around solar-type stars (Kasting et al. 1993). These differences imply that detecting Earth-mass planets in the habitable zones of M dwarfs is much less demanding in terms of Doppler precision than detecting the same planets around solar-type stars. The planetary system orbiting Gl 581 shows that detecting potentially habitable planets around M dwarfs is within the reach of current high-precision Doppler surveys.

A trio of super-Earths around HD 40307 The latest highlight from the HARPS GTO program is the planetary system discovered around the K dwarf HD 40307 (Mayor et al. 2008). This system comprises three super-Earths (minimum masses of 4.2, 6.8 and 9.2 M_{\oplus} ; periods of 4.3, 9.6 and 20.5 days), the inner planet being the lightest planet detected to date around a Sun-like star. Again,

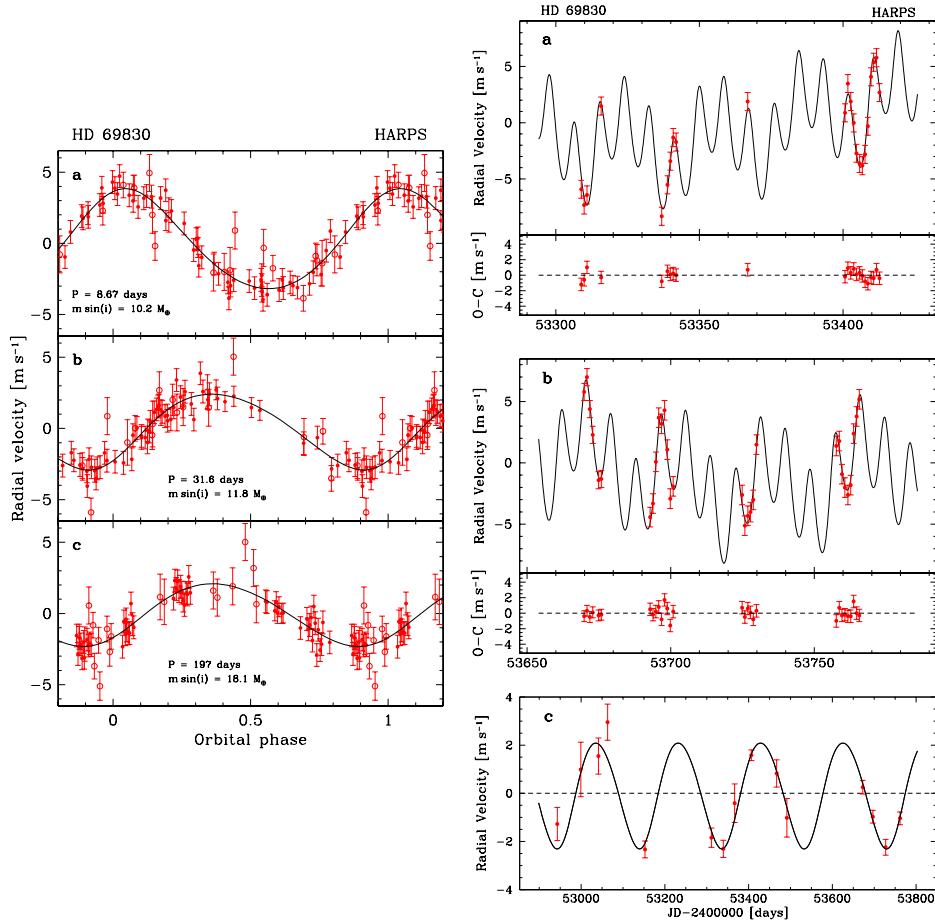


Fig. 13. *Left:* Phase-folded orbits for the three planets around HD 69830. *Right:* Radial-velocity curve as a function of time. Panels a and b show the cumulative signal of the three planets. Panel c shows the orbit of the outer planet when the observations are binned to one data point per observing run. Figures from Lovis et al. (2006).

one should note the very small semiamplitudes of the three reflex motions (2.0, 2.5, and 4.6 m s^{-1}) and the low rms of the residuals around the best-fit model (0.85 m s^{-1}).

4.2.2 Nascent statistics and emerging trends

Occurrence rate of low-mass planets The recent discoveries of planetary systems with Neptune-mass planets or super-Earths confirm that low-mass planets are common in short-period orbits around solar-type stars. A first estimate based

on the HARPS survey suggests that $30 \pm 10\%$ of the G-K dwarfs harbor a planet with $m_p \sin i < 30 M_\oplus$ and $P < 50$ days (Mayor et al. 2008).

Multiple planet systems with low-mass planets The fraction of multiple planet systems with at least one low-mass planet is very high ($\sim 80\%$). One can argue that this high value stems from an observational bias, the detection of some low-mass planets resulting from a special interest for the host star and its first-found planet(s). However, this is less and less true, and many of the recent detections are the result of systematic surveys, not of follow-up observations. The fraction of multiple planet systems with at least one low-mass planet is thus probably intrinsically high.

Mass distribution As shown in Fig. 8, the low-mass planets discovered recently seem to build up a new population which distinguishes itself from the population of giant planets. That is, the mass distribution looks bimodal and the decrease previously observed below $1 M_{\text{Jup}}$ may not be due entirely to selection effects. Remarkably, the synthesis population models of Mordasini et al. (2007) predict a planetary initial mass function which possess a local minimum near $\sim 40 M_\oplus$ ($0.13 M_{\text{Jup}}$) and a local maximum for Neptune-mass planets ($0.05 M_{\text{Jup}}$). Present data on low-mass planets are thus consistent with theoretical expectations and future discoveries will put to the test the relative overabundance of Neptune-mass planets predicted by theory.

Planet-metallicity correlation The correlation observed between the occurrence rate of giant planets and stellar metallicity seems less pronounced for low-mass planets (Udry et al. 2006; Bonfils et al. 2007). If confirmed, this trend could indicate that most of the short-period Neptune-mass planets are subcritical planetary cores rather than the remnants of evaporated giant planets. Future results from Doppler surveys and from transit observations (Sect. 5) should provide important constraints to characterize the nature and the origin of short-period Neptune-mass planets.

Stellar mass dependence M dwarfs seem to harbor more low-mass than giant planets in short-period orbits (Endl et al. 2008; Bonfils et al. 2007), implying that the ratio of Jupiter- to Neptune-mass planets may decrease with decreasing stellar mass. The sample of low-mass planets is still too small to draw robust conclusions, but again this trend is consistent with theoretical predictions (Benz et al. 2008; Ida & Lin 2005; Laughlin et al. 2004). The planet population orbiting M dwarfs is thus probably quite different from the planet population orbiting solar-type stars.

4.3 Exploring the limitations on Doppler measurements with HARPS

In the context of the GTO program, significant efforts have been put into characterizing the limitations on HARPS measurements with the aim of identifying the

main obstacles to the detection of Earth twins. The two factors that mainly limit the instrumental precision of HARPS are the stability in the illumination of the spectrograph and the wavelength calibration. To minimize variations in the illumination pattern, a specific guiding algorithm has been implemented on the ESO 3.6-m telescope. This algorithm controls the position of the photocenter at the 0.05 arcsec level, keeping the guiding noise below 30 cm s^{-1} . As to the wavelength calibration, it has been improved recently and the global uncertainty is now of 20 cm s^{-1} (Lovis & Pepe 2007).

Stellar noise is another major limitation on very high precision Doppler measurements. As shown in Fig. 7, solar-like oscillations are clearly detected with HARPS. The strategy adopted to minimize this oscillation noise consists in setting the exposure times to 10-15 minutes to average out the signal over 2-3 oscillation periods. Although time consuming, this approach allows to keep the residual noise below $\sim 50 \text{ cm s}^{-1}$ for late-G and K dwarfs. On intermediate and long time scales, Doppler measurements are affected by stellar granulation and stellar activity, respectively. The impact of stellar granulation has not been quantified precisely yet. As to stellar activity, present results indicate that well-selected quiet G-K dwarfs exhibit a jitter level below 1 m s^{-1} (Pepe & Lovis 2008). Moreover, binning the observations over time scales comparable to the rotational periods of the stars permits to significantly average out stellar noise. Proceeding in this way, a precision of $30\text{-}40 \text{ cm s}^{-1}$ has been obtained on a few test cases (e.g. HD 69830). Further work will be needed to quantify the ultimate limitation imposed by stellar activity, but a careful selection of chromospherically inactive targets probably allows to achieve a precision better than 50 cm s^{-1} on many stars.

The short-term (1 night) precision of HARPS has been characterized by asteroseismology observations of the star α Cen B carried out during the commissioning phase. Subtracting photon noise (17 cm s^{-1}) and stellar noise (44 cm s^{-1}) from the global rms of the measurements (51 cm s^{-1}) leaves 20 cm s^{-1} for all other error sources (guiding errors, instrumental errors, influence of the atmosphere, etc.). On short time scales, the precision is thus mainly limited by photon noise (targets from planet search programs are fainter than α Cen B) and by the intrinsic stability of the stars.

The long-term precision of HARPS is more difficult to characterize. The histogram of the observed radial-velocity dispersions for the stars from the high-precision GTO program (G and K dwarfs) presents a mode at 1.4 m s^{-1} (Mayor & Udry 2008). Yet, part of the observed scatter is likely caused by undetected multiple planet systems with low-amplitude Doppler signals and by stellar activity. The long-term performances of HARPS are thus probably better illustrated by considering the residuals around the best orbital solutions published so far. For several stars (e.g. HD 69830, HD 40307), these residuals are below 1 m s^{-1} , which indicates that HARPS reaches a sub- m s^{-1} precision on the long term. If reproducible on a sufficiently large sample of stars, the precision of 35 cm s^{-1} obtained for HD 69830 would show that we are not far from detecting Earth-mass planets in the habitable zones of Sun-like stars.

4.4 *Perspectives and future instruments*

The exciting results obtained with HARPS have motivated new studies to push down the limits of Doppler spectroscopy to reach the 1 cm s^{-1} precision level. From the instrumental perspective, the experience gained with HARPS indicates that reaching this precision level should be possible, though several issues will have to be solved (Pepe & Lovis 2008). From the scientific perspective, the main limitation on ultra high Doppler precision will probably be stellar noise. But again the results obtained with HARPS are encouraging, and applying an adequate observing strategy on carefully selected targets offers good prospects of averaging out stellar noise down to $10\text{-}20 \text{ cm s}^{-1}$ on short and intermediate timescales for some dozens of stars. Future ultra-stable high-resolution spectrographs are thus under study. The major European project is CODEX for the Extremely Large Telescope (Pasquini et al. 2005). CODEX aims at reaching a precision of 1 cm s^{-1} over at least 10 years to directly measure the expansion of the Universe. For planet searches, CODEX would provide an unprecedented facility for the radial-velocity follow-up of Earth-twin candidates detected through photometric transits (see next section). As an intermediate step between HARPS and CODEX, ESO foresees the realization of ESPRESSO for the Very Large Telescope (D’Odorico 2007). ESPRESSO would be a second-generation HARPS-type instrument designed to achieve a long-term precision of 10 cm s^{-1} . These characteristics would allow to carry out a systematic search for Earth-mass planets.

5 **Transiting planets**

In the course of their orbit, some extrasolar planets intersect the line of sight between the star and the observer, momentarily occulting part of the starlight. These regular passages in front of the stellar disk are called transits, while passages behind the stellar disk are called occultations⁵. For a distant observer, the probability to see a transiting geometry is low for long-period planets such as Jupiter or the Earth (0.1% and 0.5%, respectively), but is higher for close-in planets such as 51 Peg b (10%). The prospects of detecting extrasolar planets by looking for transits have thus considerably improved with the discovery of hot Jupiters. To date, 52 extrasolar planets are known to transit their parent stars. These planets are very precious because they provide us with unique information about their physical properties and atmospheres.

5.1 *Observations of planetary transits and occultations*

5.1.1 Photometric transits

Two examples of transit light curves are shown in Fig. 14. Besides their repetition time (which corresponds to the planet’s orbital period), such light curves provide

⁵Transits are sometimes called primary eclipses, while occultations are also referred to as secondary eclipses or antitransits.

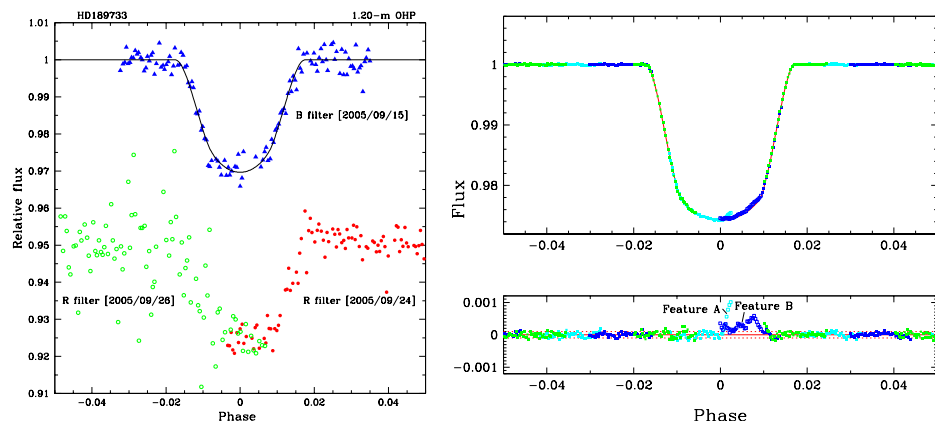


Fig. 14. Phase-folded transit light curves for HD 189733 b obtained from the ground (*left*) and from space (*right*). Features A and B observed in the residuals of the right-hand light curve are attributed to the occultation of starspots by the planet. Figures from Bouchy et al. (2005c) and Pont et al. (2007).

four observables: the transit duration, the transit depth, the ingress/egress duration, and the central curvature. These two last parameters correspond to relatively subtle features in the curves and can be measured only on high signal-to-noise data. By supplementing the transit depth, duration, and the orbital period with some external knowledge of the stellar mass and radius, we can estimate the inclination of the planetary orbit and the planet's radius (e.g. Seager & Mallén-Ornelas 2003). However, transit photometry provides no information about the planet's mass. Transit photometry and Doppler spectroscopy are thus highly complementary in their outcomes, and combined observations allow to determine both the true mass and the radius of a planet.

Transiting planets can be discovered and characterized through two different paths. In the first case, the planet detection is made through Doppler measurements and follow-up photometric observations reveal the transit. The first extra-solar planet found to transit its host star, HD 209458 b, was discovered in this way (Charbonneau et al. 2000; Henry et al. 2000; Mazeh et al. 2000). In the second case, photometric observations detect a transit and follow-up Doppler measurements confirm the planetary nature of the transiting object. Spectroscopic confirmation is essential in this case because transit photometry suffers from a high rate of false alarms (e.g. Brown 2003). Photometric detection is the most efficient channel to discover transiting planets, but the bright and nearby stars of Doppler surveys are better suited for complementary studies (Sect. 5.1.3).

The passage of Jupiter in front of the Sun (or of a Neptune-like planet in front of an M5 dwarf) produces a dip of 1% in the light curve, while a transit of the Earth produces a dip of 0.01%. Photometric transits from short-period Jupiter-sized planets can be detected from the ground, but transits from

Earth-sized planets are detectable only from space (see e.g. Brown 2008 for further details). Numerous photometric surveys searching for planetary transits are presently active and the rate of discovery has increased rapidly over the past two years. Among ground-based surveys, HAT (Bakos et al. 2007), OGLE (Udalski et al. 2002a), TrES (Alonso et al. 2004), WASP (Cameron et al. 2007), and XO (McCullough et al. 2006) have successfully detected transiting planets. These surveys typically monitor tens of thousands of stars with a photometric precision better than 10 mmag. CoRoT – the first space-borne mission largely dedicated to the discovery of planetary transits – has also found several planets since its launch in December 2006 (Barge et al. 2008). During its 2.5-year mission, CoRoT will monitor $\sim 60,000$ stars for 150 continuous days, permitting the detection of super-Earths ($\geq 2 R_{\oplus}$) and larger planets with periods below ~ 50 days (e.g. Moutou 2006).

An example of photometric follow-up: GJ 436 The low-mass planets discovered since 2004 have prompted intensified follow-up photometry to check for possible transits. The first – and currently only – Neptune-sized planet found to transit its parent star is GJ 436 b, whose transits were detected at a non-professional observatory in the Swiss Alps (Gillon et al. 2007b). This discovery opened a new window for planetary studies and triggered immediate follow-up observations with the Spitzer Space Telescope (Gillon et al. 2007a; Deming et al. 2007; Demory et al. 2007, see also Sect. 5.1.3). The mass and radius of GJ 436 b suggest an internal structure similar to that of Neptune, with a rocky core surrounded by a thick water layer and a thin gaseous envelope (Fig. 16). Nonetheless, without additional observational constraints, the internal composition of GJ 436 b cannot be determined in detail (Adams et al. 2008, see also Sect. 5.2.2).

An example of Doppler follow-up: the OGLE candidates In 2002-2003, OGLE was the first photometric survey to deliver a series of planet candidates (Udalski et al. 2002a,c,b, 2003), and Doppler follow-up programs were immediately initiated to identify genuine planets. The task was difficult, however, because most of the OGLE targets are too faint ($V \in [14;18]$) to be observed with standard planet-search spectrographs. The Geneva team resorted to using the FLAMES/UVES multi-fiber spectrograph on the Very Large Telescope (VLT) to follow up spectroscopically many of the OGLE candidates (Bouchy et al. 2005b; Pont et al. 2005). This effort has been very successful, leading to the discovery of 3 of the 5 transiting planets found among the 137 first OGLE candidates (Bouchy et al. 2004; Pont et al. 2004). The follow-up campaign has also yielded empirical occurrence rates for the main types of false alarms: transits by small stars (38%), multiple star systems (24%), false transit detections (14%), and grazing eclipses (7%). Planets represent only $\sim 7\%$ of the total number of candidates.

The follow-up of the OGLE candidates has demonstrated the necessity and the efficiency of Doppler observations in identifying genuine planets among the numerous false alarms. Yet, characterizing the transits exhibited by the faintest OGLE targets is close to being impractical. The OGLE survey is thus near the

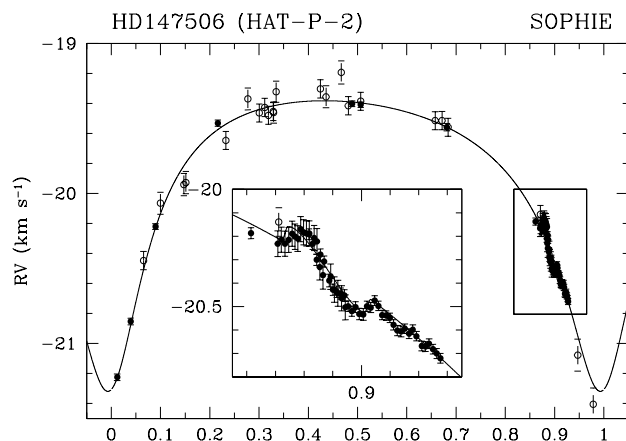


Fig. 15. Phase-folded radial-velocity curve for HD 147506 showing the Rossiter-McLaughlin effect (inset). Figure from Loeillet et al. (2008).

upper limiting magnitude for spectroscopic follow-up with existing ground-based facilities.

5.1.2 Spectroscopic transits: the Rossiter-McLaughlin effect

A planetary transit produces not only a photometric signal but also a spectroscopic signal called the Rossiter-McLaughlin effect. This anomaly in Doppler shift measurements traces the passage of the planet in front of the rotating stellar disk (Fig. 15). That is, when the planet occults part of the approaching (blueshifted) stellar hemisphere, the integrated starlight appears slightly redshifted, an effect interpreted as an anomalously high radial velocity. The reverse effect is observed when the planet occults part of the receding stellar hemisphere. For extrasolar planets, the Rossiter-McLaughlin effect was first observed and modeled for HD 209458 (Queloz et al. 2000). Since then it has been detected for 11 transiting systems (see Winn 2008 for a review). Two important parameters can be obtained by modeling the Rossiter-McLaughlin effect: the direction of planetary revolution (prograde or retrograde orbit), and the angle λ between the sky projections of the orbital and the stellar rotation axes. This angle gives us some information about the degree of alignment of the planet's orbital angular momentum vector with the stellar spin axis (spin-orbit alignment), which provides in turn an important constraint for the formation models of hot Jupiters (Sect. 5.2.3).

5.1.3 Precise monitoring of transits and occultations

Close-in planets with large planet-to-star radius ratios and transiting nearby bright stars permit a variety of follow-up studies which provide us with deeper insight into the physical properties of these planets. The two most favorable systems

for detailed studies are HD 209458 b (Henry et al. 2000; Charbonneau et al. 2000; Mazeh et al. 2000) and HD 189733 b (Bouchy et al. 2005c).

Transit light curves of extreme accuracy – as obtained with the Hubble Space Telescope, e.g. right panel of Fig. 14 – reduce the ambiguity between the estimated parameters (stellar radius, planetary radius, orbital inclination, stellar limb darkening) and yield very precise planetary radii (e.g. Brown et al. 2001; Pont et al. 2007). High-quality transit time series allow additionally to search for evidence of planetary satellites, Saturn-type rings, or additional planets (e.g. Sartoretti & Schneider 1999; Barnes & Fortney 2004; Agol et al. 2005).

Follow-up observations using the Hubble⁶ and Spitzer⁷ Space Telescopes have provided the first data on the atmospheres of extrasolar planets. At visible and ultraviolet wavelengths, the light emitted by the planet is negligible and the technique of transmission spectroscopy has been employed to study the chemical composition and the physical properties of planetary atmospheres (e.g. Brown 2001). Transit spectroscopy uses the fact that the major sources of opacity in a planetary atmosphere depend on wavelength. Due to this dependence, the planet’s effective radius – and thus the transit depth, which is the ratio of the planet-to-star surface area – vary with wavelength. Searching for relative changes in transit depth as a function of wavelength is thus a means to probe the absorption properties of a planet’s atmosphere (e.g. Charbonneau et al. 2002; Vidal-Madjar et al. 2003).

At infrared wavelengths, the planet-to-star contrast ratio improves considerably, permitting a direct detection of the photons emitted from the planet. Since hot Jupiters are believed to rotate synchronously with their orbital period (i.e. they are tidally locked), they present permanent day and night sides. The depth of the secondary eclipse (occultation) allows to characterize the day-side flux (thermal emission) from the planet (e.g. Deming et al. 2005; Charbonneau et al. 2005), while observations at various orbital phases allow to characterize the planet’s longitudinal temperature profile (e.g. Harrington et al. 2006; Knutson et al. 2007). In addition, the timing and duration of the secondary eclipse place useful constraints on the orbital eccentricity (e.g. Deming et al. 2007; Demory et al. 2007). Up to now, the thermal emission from six extrasolar planets has been detected (e.g. Charbonneau et al. 2008, and references therein).

5.2 Noteworthy results obtained from transiting planets

5.2.1 A new class of planets: the very hot Jupiters

Three of the five planets discovered among the first 137 OGLE candidates have orbital periods of ~ 1.5 days (Konacki et al. 2003; Bouchy et al. 2004), which originally placed them in an empty region of the period distribution, below the pile-up of hot Jupiters. These new planets were accordingly termed very hot Jupiters. Since the sensitivity of Doppler spectroscopy increases with decreasing period, the

⁶<http://hubble.nasa.gov>

⁷<http://www.spitzer.caltech.edu>

absence of very hot Jupiters in the discoveries of radial-velocity surveys looked surprising. Gaudi et al. (2005) showed that transit surveys are actually ~ 6 times more sensitive to planets with periods of 1 day than of 3 days, a fact that could explain the observations. Since then, Doppler surveys have found several planets with periods of 2-3 days, while transit surveys have detected many regular hot Jupiters. These discoveries have bridged the gap between the two populations and confirm that there is no significant incompatibility between the results of Doppler and transit surveys.

5.2.2 Mass-radius relationships and bulk compositions

The measurement of a planet's mass and radius give us the mean density, from which we can infer some information about the planet's bulk composition (Fig. 16). Most of the known transiting planets have densities below 1.5 g cm^{-3} , so they must be composed primarily of hydrogen and helium, like Jupiter and Saturn. Historically, this has been an important confirmation of their planetary status.

Some transiting giant planets have high densities which cannot be explained by a pure H/He composition. The most extreme case is HD 149026 b (indicated on Fig. 16), whose small radius requires the presence of $\sim 70 M_{\oplus}$ of heavy elements (2/3 of the total mass) in its interior (Sato et al. 2005). Giant planets with small radii are accounted for due to variations in the amount of heavy elements sequestered in a central core and/or distributed throughout the gaseous envelope (Guillot 2008; Burrows et al. 2007a). Since the presence of a solid core is a natural characteristic of formation by core accretion, giant planets with small radii appear to support the core accretion model. Nonetheless, if they are common, planets with 2/3 of their mass of heavy elements are a challenge to any formation model, including core accretion (Sato et al. 2005; Ikoma et al. 2006; Broeg & Wuchterl 2007).

Contrary to HD 149026 b, some giant planets such as HD 209458 b (also indicated on Fig. 16) have unexpectedly large radii and low densities. According to standard models of irradiated planets, these hot Jupiters are too big for their mass and age, a characteristic which is still unexplained (see Guillot 2008 or Burrows et al. 2007a for further details).

Low-mass planets are expected to display a wide variety of compositions and internal structures. According to theoretical predictions (e.g. Fortney et al. 2007; Seager et al. 2007), Neptune-mass planets can be composed primarily of refractory materials (rock, iron, planetary ices⁸, but also of H/He, or of a mixture of these possibilities). As to super-Earths, they are presumably composed of refractory species. It should be noted that there is some ambiguity and degeneracy in inferring bulk compositions from mean densities, especially for planets with a mass between 5 and 20 M_{\oplus} (Adams et al. 2008). For example, mass and radius measurements alone are insufficient to distinguish between an ocean planet (a planet

⁸Planetary ices comprise ammonia, methane, and water (in any phase, not necessarily solid).

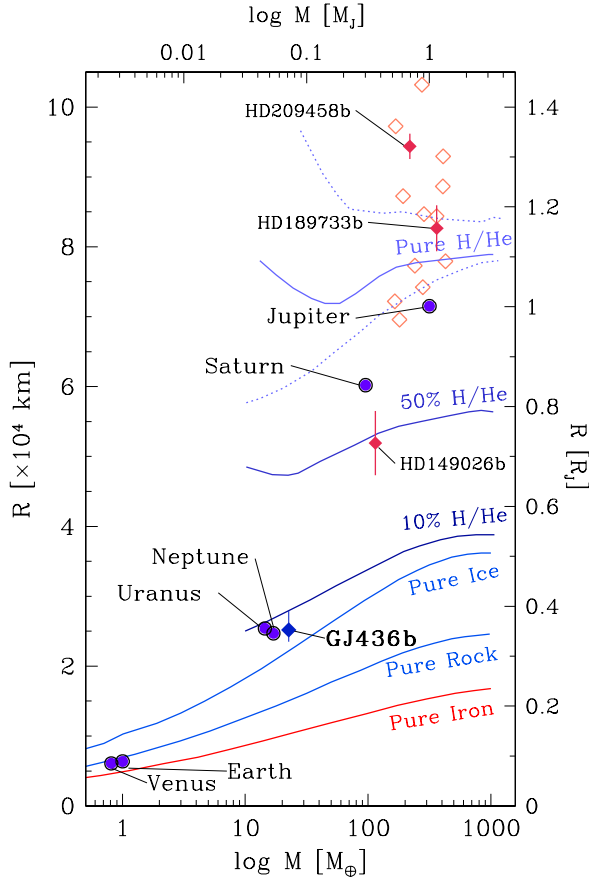


Fig. 16. Mass-radius diagram for planets. Transiting hot Jupiters (diamonds), planets from the Solar System (dots), and GJ436 b are indicated. Figure from Gillon et al. (2007b), adapted from the models of Fortney et al. (2007).

with $>25\%$ of water by mass) and a rocky planet with a massive H/He gaseous envelope.

5.2.3 Spin-orbit alignment

Rossiter-McLaughlin observations obtained so far show that in all except one case transiting planets are on prograde orbits aligned with the stellar rotation axis (see Winn 2008 for a review). These results suggest that the migration of hot Jupiters generally preserves spin-orbit alignment, an observation that disfavors scattering processes or Kozai migration as the main formation channel for hot Jupiters.

5.2.4 Planetary atmospheres

Hot Jupiters are tidally locked and receive $\gtrsim 10,000$ times more radiation from their stars than Jupiter does from the Sun. Due to this high and asymmetric irradiation, their atmospheric properties are expected to differ significantly from those of Jupiter and Saturn. Atmosphere models of hot Jupiters predict transmission spectra characterized by strong absorption lines due to the sodium and potassium resonance doublets at visible wavelengths, and by strong molecular bands of water, carbon monoxide, and methane in the infrared (e.g. Brown 2001). A significant source of uncertainty in atmosphere models is the possible presence of hazes or clouds, which can block the stellar flux at any height in the atmosphere. Another key question regarding hot Jupiters is whether atmospheric circulation efficiently redistributes the absorbed stellar radiation from the day side to the night side.

Follow-up studies on HD 209458 b have revealed the presence of sodium, hydrogen, water, and more tentatively oxygen and carbon in its atmosphere (Charbonneau et al. 2002; Vidal-Madjar et al. 2003, 2004; Barman 2007; Burrows et al. 2007b; Knutson et al. 2008b). Hydrogen absorption extends beyond the planet's Roche lobe⁹, indicating that HD 209458 b has an extended and evaporating atmosphere (see the contribution by Ehrenreich). The infrared broadband emission spectrum of HD 209458 b differs significantly from the predictions of standard atmosphere models, which was interpreted as evidence for an atmospheric temperature inversion (Knutson et al. 2008a; Burrows et al. 2007b). The day-night contrast of HD 209458 b has not been measured directly, but atmospheric circulation seems relatively efficient (Cowan et al. 2007; Knutson et al. 2008b).

Follow-up studies on HD 189733 b engendered lively discussions about the detection of water in its atmosphere (Tinetti et al. 2007; Ehrenreich et al. 2007; Beaulieu et al. 2008; Swain et al. 2008; Charbonneau et al. 2008; Barman 2008; Fortney & Marley 2007; Grillmair et al. 2007). The good agreement obtained recently between the broadband emission spectrum measured by Charbonneau et al. (2008) and the models of Barman (2008) provides convincing evidence that water absorption does shape the infrared spectrum of HD 189733 b. Methane and sodium have also been detected in its atmosphere (Swain et al. 2008; Redfield et al. 2008). The emergent spectrum of HD 189733 b is well matched by standard models which do not include an atmospheric temperature inversion (Charbonneau et al. 2008). HD 189733 b is only slightly hotter on the day side than on the night side, indicating that the energy from the irradiated hemisphere is efficiently redistributed throughout its atmosphere (Knutson et al. 2007, 2008a).

Detailed follow-up studies on HD 209458 b and HD 189733 b have thus revealed both similarities and fundamental differences in their atmospheric properties. Together with the data obtained on a few other transiting systems (see Burrows et al. 2008 for a review), the above results support the idea that the atmospheres of hot Jupiters diverge into two groups: those with and those without a temperature

⁹The Roche lobe outlines the volume surrounding an object within which material is gravitationally bound to it.

inversion (Fortney et al. 2008; Burrows et al. 2008).

5.3 *Perspectives and future instruments*

In 2009, CoRoT will be joined by the Kepler¹⁰ satellite, which will monitor 100,000 main-sequence stars for 4 continuous years to detect the transits of Earth-like planets (e.g. Basri et al. 2005). Besides the discovery of hundreds of low-mass planets, CoRoT and Kepler will provide the first measure of the occurrence of Earth- and Neptune-sized planets at short and intermediate periods. The frequency of Earth-sized planets orbiting in the habitable zones of solar-type stars is a key parameter for the design of the next generation of project missions, which will aim at characterizing the atmospheres of Earth-like planets.

Space-based transit searches do not eliminate the need for spectroscopic follow-up, but the higher quality of the photometry reduces the rate of false alarms. The radial-velocity follow-up of the CoRoT planet candidates is conducted with CORALIE, SOPHIE, HARPS, the Coudé spectrograph on the Alfred-Jensch telescope, and FLAMES/UVES for the faintest targets. The spectroscopic follow-up of the Kepler planet candidates will be much more challenging and will require a larger investment of telescope time. To perform the Doppler follow-up of interesting planet candidates identified by Kepler, the Harvard University and the Geneva Observatory have joined in a collaboration to build and operate the HARPS-N spectrograph¹¹. This improved HARPS-type instrument will be installed on the William-Herschel Telescope at La Palma Observatory in 2009. In synergy with Kepler, HARPS-N is a promising step towards the detection of rocky planets in the habitable zones of solar-type stars.

Regarding the precise monitoring of transits and occultations, Spitzer will run out of cryogen in spring 2009, which will eliminate its ability to observe at wavelengths longer than 4.5 μm . An extended “warm” Spitzer mission has been proposed, in which the spacecraft would continue to operate (at the same sensitivity) in the two shortest wavelength channels. Unlike Spitzer, Hubble should be reborn with the servicing mission scheduled for early 2009. Beyond Hubble and Spitzer, we will have to wait the launch of the James Webb Space Telescope¹² in the middle of the next decade to continue and extend the study of extrasolar planetary atmospheres.

6 Conclusion and perspectives

For centuries, our knowledge of planetary systems has been based on a single example, the Solar System. During the last thirteen years, Doppler spectroscopy has allowed the detection of ~ 300 extrasolar planets, opening a new window on planetary sciences. These discoveries have considerably broadened our appreciation

¹⁰<http://kepler.nasa.gov>

¹¹http://obswww.unige.ch/Instruments/harps_north

¹²<http://www.jwst.nasa.gov>

of the diversity of possible planetary systems and have revolutionized our ideas about planet formation.

By the standards of the Solar System, many extrasolar planets exhibit singular properties, including very short orbital periods, high eccentricities, and large masses. Stars of different masses seem to harbor different planet populations and multiple planet systems appear to be the rule. For solar-type stars, stellar metallicity is a strong predictor of the presence of giant planets in the inner regions of the system. Migration via tidal interaction with the gaseous protoplanetary disk appears to play a central role in the formation and early evolution of these giant planets. Some extrasolar planets were found in environments relatively hostile to their presence (pulsars, spectroscopic binaries), indicating that planet formation is a robust process. The recent discoveries of Neptune-mass planets and super-Earths at close (Doppler spectroscopy) and intermediate (microlensing) separations support the theoretical prediction that low-mass planets are more numerous than their giant cousins.

Transiting planets are only a small subset of all extrasolar planetary systems, but they offer an unique opportunity to deepen our understanding of planet structure and composition. With the exception of one hot Neptune, transiting planets are gas giants with a wide range of masses and radii. Follow-up observations using the Hubble and Spitzer Space Telescopes provided the first glimpse into the atmospheres of some hot Jupiters, and the first detections of photons emitted from extrasolar planets. Planetary emission spectra reveal fundamental differences in atmospheric properties, leading to the suggestion that the irradiated atmospheres of hot Jupiters bifurcate into two groups.

The above observations provide an ever-growing database with which planet formation theories can be put to the test. By combining observed properties of protoplanetary disks, models of planet formation and evolution, and observational selection effects, theorists now generate in a self-consistent way synthetic planet populations which can be compared with the actual detections. Recent models based on the core accretion paradigm successfully reproduce key observational features such as the mass distribution and the planet-metallicity correlation. Although much remains to be understood about planet formation, these new theoretical achievements reinforce the idea that most of the known planets formed through core accretion.

To progress in our understanding of planet formation and to appreciate the significance of our Earth, we must detect a wide range of planetary systems, including planets and host stars both similar and dissimilar to our own. This can be achieved through two different paths: by further developing existing techniques to increase their capabilities, and by developing new techniques to explore different regions of the parameter space. The characterization of transiting planets illustrates the benefit of combining the results obtained with two different observational techniques.

As we have seen, Doppler spectroscopy has reached neither its instrumental nor its astrophysical limits. The latter will probably be dominant, but applying an adequate strategy on carefully selected targets offers good prospects of averag-

ing out stellar noise down to $10\text{-}20\text{ cm s}^{-1}$ on short and intermediate time scales for some dozens of stars. The next generation of HARPS-type instruments aiming at a Doppler precision of $10\text{-}20\text{ cm s}^{-1}$ (HARPS-N, the ESPRESSO project) should therefore be able to detect Earth-mass planets in short-period orbits, and to characterize some of these planets up to periods of ~ 1 year. Ultra-stable spectrographs aiming at a Doppler precision of 1 cm s^{-1} should be technically feasible. If stellar noise permits, such instruments would allow the detection and the precise characterization of Earth twins.

While Doppler spectroscopy is intrinsically sensitive to short-period planets, astrometry and direct imaging are particularly suited to detect planets in wide orbits. Up to now, these two techniques have very marginally contributed to planetary studies, but this is going to change thanks to the upcoming deployment of new facilities. In 2009, the PRIMA¹³ instrument for the VLT interferometer should become fully operational, allowing the astrometric detection of planets down to the mass of Neptune in the separation range 1-5 AU (Launhardt et al. 2008). From space, the GAIA¹⁴ mission (scheduled for launch in 2011) will detect thousands of extrasolar planets, revolutionizing the database of extrasolar planets with known orbital elements and masses (Casertano et al. 2008). Although astrometric observations are sufficient to determine three-dimensional orbits and true planetary masses, additional Doppler measurements will be of great help in constraining the large number of free parameters, especially for multiple planet systems. Regarding direct imaging, a few “extreme” adaptive optics systems are under construction, including SPHERE for the VLT (Beuzit et al. 2008) and GPI for the Gemini Observatory (Macintosh et al. 2008). Starting in ~ 2011 , these instruments will detect, characterize the atmospheres, and determine the radii of wide ($\sim 5\text{-}100$ AU) and massive ($\gtrsim 1\text{-}5 M_{\text{Jup}}$) planets of various ages ($\sim 10\text{-}1000$ Myr). All together, these upcoming facilities will probe the intermediate and outer regions of protoplanetary disks, providing new information about the formation, evolution, and migration of giant planets.

Doppler spectroscopy and microlensing have opened the way to the detection of low-mass planets, and mature detection techniques now aim at identifying an Earth-mass planet located in the habitable zone of its host star. Microlensing surveys can yield the frequency of such planets, but they do not allow a precise characterization of their planet candidates (e.g. Beaulieu et al. 2008). Space-based transit photometry is presently the most sensitive method for planetary detection, and the pending Kepler mission offers good prospects of finding the first Earth-sized planet potentially habitable. Yet, Doppler spectroscopy is a serious competitor, and it may win the race. In any case, both techniques will play a key role in detecting and characterizing Earth-mass planets in the near future. Due to their ubiquity and low mass, M dwarfs are ideal targets for the detection of terrestrial planets. In addition to optical radial velocities, infrared Doppler spectroscopy represents an attractive new technique to search for and characterize planets around

¹³<http://obswww.unige.ch/Instruments/PRIMA>

¹⁴<http://gaia.esa.int/science-e/www/area/index.cfm?fareaid=26>

late-type ($\gtrsim M4$) M dwarfs (e.g. Martín et al. 2005 or the SPIRou project¹⁵). In the more distant future, space-borne astrometry could contribute to the detection of low-mass planets as well. The SIM Lite¹⁶ project would serve this purpose (e.g. Tanner et al. 2006), but its future is highly uncertain.

If it is approved, the warm Spitzer mission will allow the community to retain the ability to characterize the atmospheres of some transiting planets for a few more years. In the middle of the next decade, JWST will take over and will allow to study the atmospheres of Earth-sized planets located in the habitable zones of main-sequence stars. On a longer time scale, infrared space interferometers could be built to directly image potentially habitable Earth-like planets and to search for life signatures in their atmospheres.

In summary, Doppler spectroscopy will continue to serve as a front-line detection technique for the next years. It will additionally provide an increasingly important support to alternative planet search techniques, in particular transit photometry and astrometry. The golden age of radial velocities is thus far from its end and Doppler spectroscopy promises additional exciting results to come.

References

- Adams, E. R., Seager, S., & Elkins-Tanton, L. 2008, *ApJ*, 673, 1160
- Agol, E., Steffen, J., Sari, R., & Clarkson, W. 2005, *MNRAS*, 359, 567
- Alibert, Y., Baraffe, I., Benz, W., et al. 2006, *A&A*, 455, L25
- Alibert, Y., Mordasini, C., Benz, W., & Winisdoerffer, C. 2005, *A&A*, 434, 343
- Alonso, R., Brown, T. M., Torres, G., et al. 2004, *ApJ*, 613, L153
- Armitage, P. J. 2007, *ApJ*, 665, 1381
- Bakos, G. Á., Noyes, R. W., Kovács, G., et al. 2007, *ApJ*, 656, 552
- Baraffe, I., Alibert, Y., Chabrier, G., & Benz, W. 2006, *A&A*, 450, 1221
- Baranne, A., Queloz, D., Mayor, M., et al. 1996, *A&AS*, 119, 373
- Barge, P., Baglin, A., Auvergne, M., et al. 2008, *A&A*, 482, L17
- Barman, T. 2007, *ApJ*, 661, L191
- Barman, T. S. 2008, *ApJ*, 676, L61
- Barnes, J. W. & Fortney, J. J. 2004, *ApJ*, 616, 1193
- Basri, G., Borucki, W. J., & Koch, D. 2005, *New Astronomy Review*, 49, 478

¹⁵http://www.ast.obs-mip.fr/article.php3?id_article=637

¹⁶http://planetquest.jpl.nasa.gov/SIMLite/sim_index.cfm

- Beaulieu, J. P., Carey, S., Ribas, I., & Tinetti, G. 2008, *ApJ*, 677, 1343
- Beichman, C. A., Bryden, G., Gautier, T. N., et al. 2005, *ApJ*, 626, 1061
- Benz, W., Mordasini, C., Alibert, Y., & Naef, D. 2006, in Tenth Anniversary of 51 Peg-b: Status of and prospects for hot Jupiter studies, ed. L. Arnold, F. Bouchy, & C. Moutou, 24–34
- Benz, W., Mordasini, C., Alibert, Y., & Naef, D. 2008, *Physica Scripta Volume T*, 130, 014022
- Beuzit, J.-L., Feldt, M., Dohlen, K., et al. 2008, in Society of Photo-Optical Instrumentation Engineers (SPIE) Conference Series, Vol. 7014
- Beuzit, J.-L., Mouillet, D., Oppenheimer, B. R., & Monnier, J. D. 2007, in Protostars and Planets V, ed. B. Reipurth, D. Jewitt, & K. Keil, 717–732
- Bodenheimer, P., Hubickyj, O., & Lissauer, J. J. 2000, *Icarus*, 143, 2
- Bonfils, X., Forveille, T., Delfosse, X., et al. 2005, *A&A*, 443, L15
- Bonfils, X., Mayor, M., Delfosse, X., et al. 2007, *A&A*, 474, 293
- Boss, A. P. 2002, *ApJ*, 567, L149
- Bouchy, F., Bazot, M., Santos, N. C., Vauclair, S., & Sosnowska, D. 2005a, *A&A*, 440, 609
- Bouchy, F., Pepe, F., & Queloz, D. 2001, *A&A*, 374, 733
- Bouchy, F., Pont, F., Melo, C., et al. 2005b, *A&A*, 431, 1105
- Bouchy, F., Pont, F., Santos, N. C., et al. 2004, *A&A*, 421, L13
- Bouchy, F., Udry, S., Mayor, M., et al. 2005c, *A&A*, 444, L15
- Bouchy, F., Udry, S., Moutou, C., et al. 2007, in , 377
- Broeg, C. & Wuchterl, G. 2007, *MNRAS*, 376, L62
- Brown, T. M. 1990, in Astronomical Society of the Pacific Conference Series, Vol. 8, CCDs in astronomy, ed. G. H. Jacoby, 335–344
- Brown, T. M. 2001, *ApJ*, 553, 1006
- Brown, T. M. 2003, *ApJ*, 593, L125
- Brown, T. M. 2008, in Extrasolar Planets, ed. H. J. Deeg, J. A. Belmonte, & A. Aparicio, 65–88
- Brown, T. M., Charbonneau, D., Gilliland, R. L., Noyes, R. W., & Burrows, A. 2001, *ApJ*, 552, 699

- Brunini, A. & Cionco, R. G. 2005, *Icarus*, 177, 264
- Burrows, A., Budaj, J., & Hubeny, I. 2008, *ApJ*, 678, 1436
- Burrows, A., Hubeny, I., Budaj, J., & Hubbard, W. B. 2007a, *ApJ*, 661, 502
- Burrows, A., Hubeny, I., Budaj, J., Knutson, H. A., & Charbonneau, D. 2007b, *ApJ*, 668, L171
- Butler, R. P., Marcy, G. W., Williams, E., et al. 1996, *PASP*, 108, 500
- Butler, R. P., Tinney, C. G., Marcy, G. W., et al. 2001, *ApJ*, 555, 410
- Butler, R. P., Vogt, S. S., Marcy, G. W., et al. 2004, *ApJ*, 617, 580
- Butler, R. P., Wright, J. T., Marcy, G. W., et al. 2006, *ApJ*, 646, 505
- Cameron, A. C., Bouchy, F., Hébrard, G., et al. 2007, *MNRAS*, 375, 951
- Campbell, B. & Walker, G. A. H. 1979, *PASP*, 91, 540
- Campbell, B., Walker, G. A. H., & Yang, S. 1988, *ApJ*, 331, 902
- Casertano, S., Lattanzi, M. G., Sozzetti, A., et al. 2008, *A&A*, 482, 699
- Charbonneau, D., Allen, L. E., Megeath, S. T., et al. 2005, *ApJ*, 626, 523
- Charbonneau, D., Brown, T. M., Burrows, A., & Laughlin, G. 2007, in *Protostars and Planets V*, ed. B. Reipurth, D. Jewitt, & K. Keil, 701–716
- Charbonneau, D., Brown, T. M., Latham, D. W., & Mayor, M. 2000, *ApJ*, 529, L45
- Charbonneau, D., Brown, T. M., Noyes, R. W., & Gilliland, R. L. 2002, *ApJ*, 568, 377
- Charbonneau, D., Knutson, H. A., Barman, T., et al. 2008, *ApJ*, 686, 1341
- Chiang, E. I., Tabachnik, S., & Tremaine, S. 2001, *AJ*, 122, 1607
- Connes, P. 1985, *Ap&SS*, 110, 211
- Cowan, N. B., Agol, E., & Charbonneau, D. 2007, *MNRAS*, 379, 641
- Cumming, A., Butler, R. P., Marcy, G. W., et al. 2008, *PASP*, 120, 531
- Cumming, A., Marcy, G. W., & Butler, R. P. 1999, *ApJ*, 526, 890
- da Silva, R., Udry, S., Bouchy, F., et al. 2006, *A&A*, 446, 717
- Delfosse, X., Forveille, T., Mayor, M., et al. 1998, *A&A*, 338, L67
- Deming, D., Harrington, J., Laughlin, G., et al. 2007, *ApJ*, 667, L199

- Deming, D., Seager, S., Richardson, L. J., & Harrington, J. 2005, *Nature*, 434, 740
- Demory, B.-O., Gillon, M., Barman, T., et al. 2007, *A&A*, 475, 1125
- Desidera, S. & Barbieri, M. 2007, *A&A*, 462, 345
- Desort, M., Lagrange, A.-M., Galland, F., Udry, S., & Mayor, M. 2007, *A&A*, 473, 983
- D'Odorico, V. 2007, *Memorie della Societa Astronomica Italiana*, 78, 712
- Duquennoy, A., Mayor, M., & Halbwachs, J.-L. 1991, *A&AS*, 88, 281
- Durisen, R. H., Boss, A. P., Mayer, L., et al. 2007, in *Protostars and Planets V*, ed. B. Reipurth, D. Jewitt, & K. Keil, 607–622
- Eggenberger, A. & Udry, S. 2007, *ArXiv e-prints*, 705
- Eggenberger, A., Udry, S., & Mayor, M. 2003, in *Scientific Frontiers in Research on Extrasolar Planets*, ed. D. Deming & S. Seager, Vol. 294, 43–46
- Eggenberger, A., Udry, S., & Mayor, M. 2004, *A&A*, 417, 353
- Ehrenreich, D., Hébrard, G., Lecavelier des Etangs, A., et al. 2007, *ApJ*, 668, L179
- Endl, M., Cochran, W. D., Kürster, M., et al. 2006, *ApJ*, 649, 436
- Endl, M., Cochran, W. D., Tull, R. G., & MacQueen, P. J. 2003, *AJ*, 126, 3099
- Endl, M., Cochran, W. D., Wittenmyer, R. A., & Boss, A. P. 2008, *ApJ*, 673, 1165
- Endl, M., Kürster, M., Els, S., et al. 2002, *A&A*, 392, 671
- Fabrycky, D. & Tremaine, S. 2007, *ApJ*, 669, 1298
- Fischer, D. A., Laughlin, G., Butler, P., et al. 2005, *ApJ*, 620, 481
- Fischer, D. A., Laughlin, G., Marcy, G. W., et al. 2006, *ApJ*, 637, 1094
- Fischer, D. A., Marcy, G. W., Butler, R. P., et al. 2008, *ApJ*, 675, 790
- Fischer, D. A. & Valenti, J. 2005, *ApJ*, 622, 1102
- Ford, E. B., Lystad, V., & Rasio, F. A. 2005, *Nature*, 434, 873
- Ford, E. B. & Rasio, F. A. 2006, *ApJ*, 638, L45
- Ford, E. B. & Rasio, F. A. 2007, *ArXiv Astrophysics e-prints*
- Fortney, J. J., Lodders, K., Marley, M. S., & Freedman, R. S. 2008, *ApJ*, 678, 1419
- Fortney, J. J. & Marley, M. S. 2007, *ApJ*, 666, L45

- Fortney, J. J., Marley, M. S., & Barnes, J. W. 2007, *ApJ*, 659, 1661
- Forveille, T., Bonfils, X., Delfosse, X., et al. 2008, *ArXiv e-prints*
- Frink, S., Mitchell, D. S., Quirrenbach, A., et al. 2002, *ApJ*, 576, 478
- Galland, F., Lagrange, A.-M., Udry, S., et al. 2005, *A&A*, 443, 337
- Gaudi, B. S. 2007, *ArXiv e-prints*, 711
- Gaudi, B. S., Seager, S., & Mallen-Ornelas, G. 2005, *ApJ*, 623, 472
- Gillon, M., Demory, B.-O., Barman, T., et al. 2007a, *A&A*, 471, L51
- Gillon, M., Pont, F., Demory, B.-O., et al. 2007b, *A&A*, 472, L13
- Gonzalez, G. 1997, *MNRAS*, 285, 403
- Griffin, R. & Griffin, R. 1973, *MNRAS*, 162, 243
- Grillmair, C. J., Charbonneau, D., Burrows, A., et al. 2007, *ApJ*, 658, L115
- Gu, P.-G., Lin, D. N. C., & Bodenheimer, P. H. 2003, *ApJ*, 588, 509
- Guillot, T. 2008, *Physica Scripta Volume T*, 130, 014023
- Halbwachs, J. L., Mayor, M., & Udry, S. 2005, *A&A*, 431, 1129
- Harrington, J., Hansen, B. M., Luszcz, S. H., et al. 2006, *Science*, 314, 623
- Hatzes, A. P., Guenther, E. W., Endl, M., et al. 2005, *A&A*, 437, 743
- Henry, G. W., Marcy, G. W., Butler, R. P., & Vogt, S. S. 2000, *ApJ*, 529, L41
- Ida, S. & Lin, D. N. C. 2004a, *ApJ*, 604, 388
- Ida, S. & Lin, D. N. C. 2004b, *ApJ*, 616, 567
- Ida, S. & Lin, D. N. C. 2005, *ApJ*, 626, 1045
- Ikoma, M., Guillot, T., Genda, H., Tanigawa, T., & Ida, S. 2006, *ApJ*, 650, 1150
- Israelian, G., Santos, N. C., Mayor, M., & Rebolo, R. 2001, *Nature*, 411, 163
- Johnson, J. A., Butler, R. P., Marcy, G. W., et al. 2007, *ApJ*, 670, 833
- Johnson, J. A., Marcy, G. W., Fischer, D. A., et al. 2006, *ApJ*, 652, 1724
- Jones, H. R. A., Paul Butler, R., Marcy, G. W., et al. 2002, *MNRAS*, 337, 1170
- Jorissen, A., Mayor, M., & Udry, S. 2001, *A&A*, 379, 992
- Kasting, J. F., Whitmire, D. P., & Reynolds, R. T. 1993, *Icarus*, 101, 108

- Kennedy, G. M. & Kenyon, S. J. 2008, *ApJ*, 673, 502
- Kley, W. 2000, in *IAU Symposium*, Vol. 200, *IAU Symposium*, 211P
- Kley, W., Lee, M. H., Murray, N., & Peale, S. J. 2005, *A&A*, 437, 727
- Knutson, H. A., Charbonneau, D., Allen, L. E., Burrows, A., & Megeath, S. T. 2008a, *ApJ*, 673, 526
- Knutson, H. A., Charbonneau, D., Allen, L. E., et al. 2007, *Nature*, 447, 183
- Knutson, H. A., Charbonneau, D., Cowan, N. B., et al. 2008b, *ArXiv e-prints*
- Konacki, M., Torres, G., Jha, S., & Sasselov, D. D. 2003, *Nature*, 421, 507
- Kuchner, M. J. & Lecar, M. 2002, *ApJ*, 574, L87
- Laughlin, G., Bodenheimer, P., & Adams, F. C. 2004, *ApJ*, 612, L73
- Launhardt, R., Queloz, D., Henning, T., et al. 2008, in *Society of Photo-Optical Instrumentation Engineers (SPIE) Conference Series*, Vol. 7013
- Lee, M. H. 2004, *ApJ*, 611, 517
- Lin, D. N. C., Bodenheimer, P., & Richardson, D. C. 1996, *Nature*, 380, 606
- Lissauer, J. J. & Stevenson, D. J. 2007, in *Protostars and Planets V*, ed. B. Reipurth, D. Jewitt, & K. Keil, 591–606
- Livio, M. & Pringle, J. E. 2003, *MNRAS*, 346, L42
- Loeillet, B., Shporer, A., Bouchy, F., et al. 2008, *A&A*, 481, 529
- Lovis, C. & Mayor, M. 2007, *A&A*, 472, 657
- Lovis, C., Mayor, M., Pepe, F., et al. 2006, *Nature*, 441, 305
- Lovis, C. & Pepe, F. 2007, *A&A*, 468, 1115
- Macintosh, B. A., Graham, J. R., Palmer, D. W., et al. 2008, in *Society of Photo-Optical Instrumentation Engineers (SPIE) Conference Series*, Vol. 7015
- Marcy, G., Butler, R. P., Fischer, D., et al. 2005a, *Progress of Theoretical Physics Supplement*, 158, 24
- Marcy, G. W. & Benitz, K. J. 1989, *ApJ*, 344, 441
- Marcy, G. W. & Butler, R. P. 1992, *PASP*, 104, 270
- Marcy, G. W. & Butler, R. P. 1998, *ARA&A*, 36, 57
- Marcy, G. W., Butler, R. P., Vogt, S. S., et al. 2005b, *ApJ*, 619, 570

- Martín, E. L., Guenther, E., Barrado y Navascués, D., et al. 2005, *Astronomische Nachrichten*, 326, 1015
- Mayor, M., Pepe, F., Queloz, D., et al. 2003, *The Messenger*, 114, 20
- Mayor, M. & Queloz, D. 1995, *Nature*, 378, 355
- Mayor, M. & Udry, S. 2008, *Physica Scripta Volume T*, 130, 014010
- Mayor, M., Udry, S., Lovis, C., et al. 2008, *ArXiv e-prints*, 806
- Mazeh, T., Naef, D., Torres, G., et al. 2000, *ApJ*, 532, L55
- McArthur, B. E., Endl, M., Cochran, W. D., et al. 2004, *ApJ*, 614, L81
- McCullough, P. R., Stys, J. E., Valenti, J. A., et al. 2006, *ApJ*, 648, 1228
- Mordasini, C., Alibert, Y., Benz, W., & Naef, D. 2007, *ArXiv e-prints*, 710
- Moutou, C. 2006, in *Tenth Anniversary of 51 Peg-b: Status of and prospects for hot Jupiter studies*, ed. L. Arnold, F. Bouchy, & C. Moutou, 342–349
- Murray, N., Hansen, B., Holman, M., & Tremaine, S. 1998, *Science*, 279, 69
- Muterspaugh, M. W., Konacki, M., Lane, B. F., & Pfahl, E. 2007, *ArXiv e-prints*
- Naef, D., Mayor, M., Beuzit, J.-L., et al. 2005, in *13th Cambridge Workshop on Cool Stars*, ed. F. Favata, G. A. J. Hussain, & B. Battrock, Vol. 560, 833
- Nagasawa, M., Ida, S., & Bessho, T. 2008, *ApJ*, 678, 498
- Nagasawa, M., Thommes, E. W., Kenyon, S. J., Bromley, B. C., & Lin, D. N. C. 2007, in *Protostars and Planets V*, ed. B. Reipurth, D. Jewitt, & K. Keil, 639–654
- Niedzielski, A., Konacki, M., Wolszczan, A., et al. 2007, *ApJ*, 669, 1354
- Noyes, R. W., Hartmann, L. W., Baliunas, S. L., Duncan, D. K., & Vaughan, A. H. 1984, *ApJ*, 279, 763
- Palmer, B. A. & Engleman, R. 1983, *Atlas of the Thorium spectrum (LA, Los Alamos: National Laboratory, —c1983)*
- Pasquini, L., Cristiani, S., Dekker, H., et al. 2005, *The Messenger*, 122, 10
- Pasquini, L., Döllinger, M. P., Weiss, A., et al. 2007, *A&A*, 473, 979
- Pätzold, M. & Rauer, H. 2002, *ApJ*, 568, L117
- Paulson, D. B., Cochran, W. D., & Hatzes, A. P. 2004, *AJ*, 127, 3579
- Pepe, F., Correia, A. C. M., Mayor, M., et al. 2007, *A&A*, 462, 769

- Pepe, F., Mayor, M., Galland, F., et al. 2002a, *A&A*, 388, 632
- Pepe, F., Mayor, M., Rupprecht, G., et al. 2002b, *The Messenger*, 110, 9
- Pepe, F. A. & Lovis, C. 2008, *Physica Scripta Volume T*, 130, 014007
- Perrier, C., Sivan, J.-P., Naef, D., et al. 2003, *A&A*, 410, 1039
- Pinotti, R., Arany-Prado, L., Lyra, W., & Porto de Mello, G. F. 2005, *MNRAS*, 364, 29
- Pinsonneault, M. H., DePoy, D. L., & Coffee, M. 2001, *ApJ*, 556, L59
- Pont, F., Bouchy, F., Melo, C., et al. 2005, *A&A*, 438, 1123
- Pont, F., Bouchy, F., Queloz, D., et al. 2004, *A&A*, 426, L15
- Pont, F., Gilliland, R. L., Moutou, C., et al. 2007, *A&A*, 476, 1347
- Queloz, D., Henry, G. W., Sivan, J. P., et al. 2001, *A&A*, 379, 279
- Queloz, D., Mayor, M., Weber, L., et al. 2000, *A&A*, 354, 99
- Raghavan, D., Henry, T. J., Mason, B. D., et al. 2006, *ApJ*, 646, 523
- Rasio, F. A., Tout, C. A., Lubow, S. H., & Livio, M. 1996, *ApJ*, 470, 1187
- Redfield, S., Endl, M., Cochran, W. D., & Koesterke, L. 2008, *ApJ*, 673, L87
- Rivera, E. J., Lissauer, J. J., Butler, R. P., et al. 2005, in *Bulletin of the American Astronomical Society*, Vol. 37, 1487
- Rupprecht, G., Pepe, F., Mayor, M., et al. 2004, in *Ground-based Instrumentation for Astronomy*, ed. A. F. M. Moorwood & M. Iye, 148–159
- Saar, S. H., Butler, R. P., & Marcy, G. W. 1998, *ApJ*, 498, L153+
- Saar, S. H. & Donahue, R. A. 1997, *ApJ*, 485, 319
- Santos, N. C., Bouchy, F., Mayor, M., et al. 2004a, *A&A*, 426, L19
- Santos, N. C., Israelian, G., & Mayor, M. 2000a, *A&A*, 363, 228
- Santos, N. C., Israelian, G., & Mayor, M. 2004b, *A&A*, 415, 1153
- Santos, N. C., Israelian, G., Mayor, M., Rebolo, R., & Udry, S. 2003, *A&A*, 398, 363
- Santos, N. C., Mayor, M., Naef, D., et al. 2000b, *A&A*, 361, 265
- Santos, N. C., Mayor, M., Naef, D., et al. 2002, *A&A*, 392, 215
- Sartoretti, P. & Schneider, J. 1999, *A&AS*, 134, 553

- Sato, B., Kambe, E., Takeda, Y., et al. 2005, PASJ, 57, 97
- Seager, S., Kuchner, M., Hier-Majumder, C. A., & Militzer, B. 2007, ApJ, 669, 1279
- Seager, S. & Mallén-Ornelas, G. 2003, ApJ, 585, 1038
- Selsis, F., Kasting, J. F., Levrard, B., et al. 2007, A&A, 476, 1373
- Setiawan, J., Pasquini, L., da Silva, L., von der Lühe, O., & Hatzes, A. 2003, A&A, 397, 1151
- Sozzetti, A. 2004, MNRAS, 354, 1194
- Stepinski, T. F. & Black, D. C. 2000, A&A, 356, 903
- Swain, M. R., Vasisht, G., & Tinetti, G. 2008, Nature, 452, 329
- Takeda, Y., Sato, B., & Murata, D. 2008, PASJ, 60, 781
- Tamuz, O., Ségransan, D., Udry, S., et al. 2008, A&A, 480, L33
- Tanner, A. M., Catanzarite, J., & Shao, M. 2006, in Society of Photo-Optical Instrumentation Engineers (SPIE) Conference Series, Vol. 6268
- Tinetti, G., Vidal-Madjar, A., Liang, M.-C., et al. 2007, Nature, 448, 169
- Tinney, C. G., Butler, R. P., Marcy, G. W., et al. 2005, ApJ, 623, 1171
- Trilling, D. E., Benz, W., Guillot, T., et al. 1998, ApJ, 500, 428
- Udalski, A., Paczynski, B., Zebrun, K., et al. 2002a, Acta Astronomica, 52, 1
- Udalski, A., Pietrzynski, G., Szymanski, M., et al. 2003, Acta Astronomica, 53, 133
- Udalski, A., Szewczyk, O., Zebrun, K., et al. 2002b, Acta Astronomica, 52, 317
- Udalski, A., Zebrun, K., Szymanski, M., et al. 2002c, Acta Astronomica, 52, 115
- Udry, S., Fischer, D., & Queloz, D. 2007, in Protostars and Planets V, ed. B. Reipurth, D. Jewitt, & K. Keil, 685–699
- Udry, S., Mayor, M., Benz, W., et al. 2006, A&A, 447, 361
- Udry, S., Mayor, M., Naef, D., et al. 2002, A&A, 390, 267
- Udry, S., Mayor, M., Naef, D., et al. 2000, A&A, 356, 590
- Udry, S. & Santos, N. C. 2007, ARA&A, 45, 397
- Valenti, J. A., Butler, R. P., & Marcy, G. W. 1995, PASP, 107, 966

- Vidal-Madjar, A., Désert, J.-M., Lecavelier des Etangs, A., et al. 2004, *ApJ*, 604, L69
- Vidal-Madjar, A., Lecavelier des Etangs, A., Désert, J.-M., et al. 2003, *Nature*, 422, 143
- von Bloh, W., Bounama, C., Cuntz, M., & Franck, S. 2007, *A&A*, 476, 1365
- Winn, J. N. 2008, *ArXiv e-prints*
- Wittenmyer, R. A., Endl, M., Cochran, W. D., et al. 2006, *AJ*, 132, 177
- Wolszczan, A. 1997, *Celestial Mechanics and Dynamical Astronomy*, 68, 13
- Wolszczan, A. & Frail, D. A. 1992, *Nature*, 355, 145
- Wright, J. T. 2005, *PASP*, 117, 657
- Wright, J. T., Marcy, G. W., Butler, R. P., et al. 2008, *ApJ*, 683, L63
- Wright, J. T., Marcy, G. W., Fischer, D. A., et al. 2007, *ApJ*, 657, 533
- Wu, Y. & Murray, N. 2003, *ApJ*, 589, 605
- Zucker, S. & Mazeh, T. 2001, *ApJ*, 562, 1038
- Zucker, S. & Mazeh, T. 2002, *ApJ*, 568, L113
- Zucker, S., Mazeh, T., Santos, N. C., Udry, S., & Mayor, M. 2003, *A&A*, 404, 775